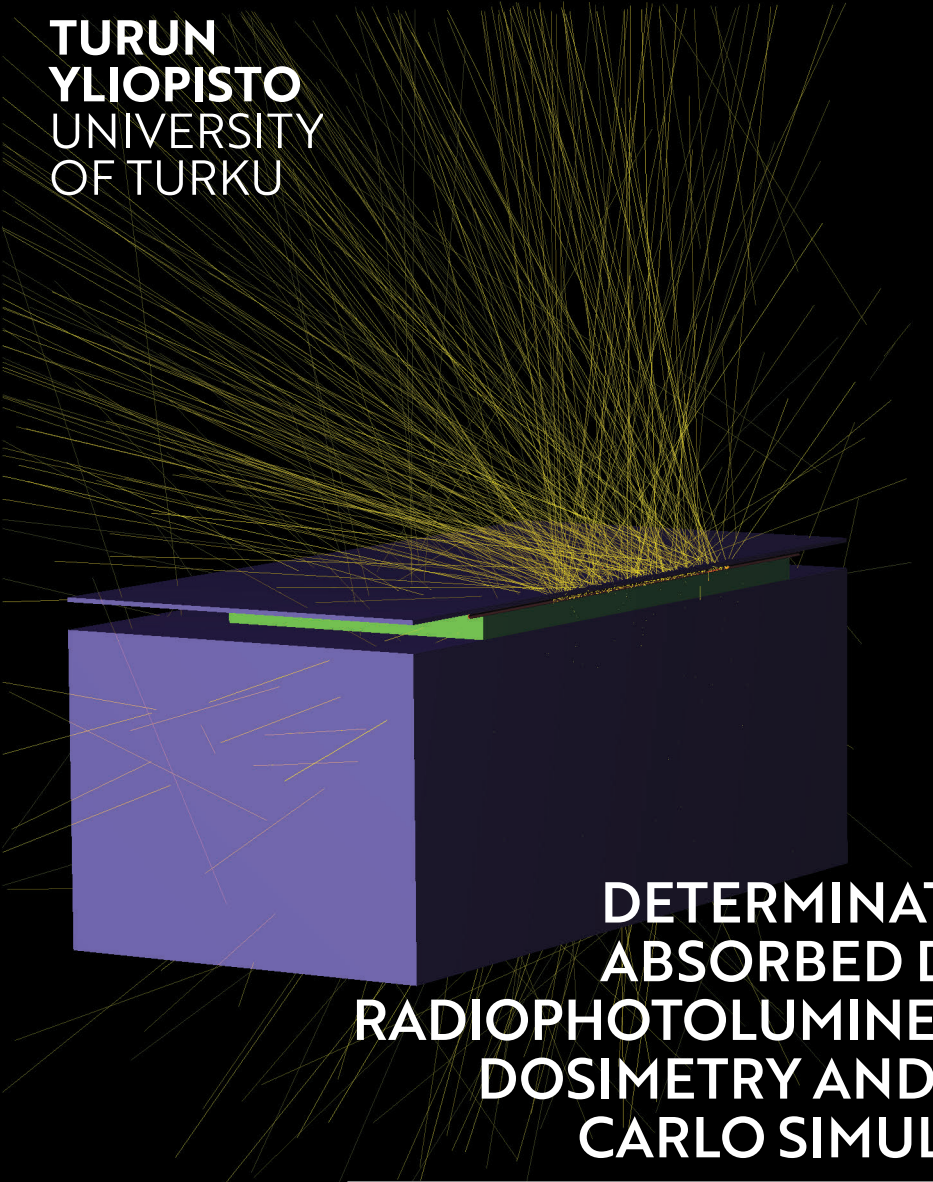




**TURUN  
YLIOPISTO  
UNIVERSITY  
OF TURKU**

A 3D visualization of particle tracks, likely from a Monte Carlo simulation. The tracks are represented by numerous thin, yellow-green lines that originate from a central point and radiate outwards in all directions. The tracks are concentrated in a rectangular volume, which is rendered in a dark blue color. The tracks appear to be entering and exiting the volume, illustrating the complex paths of particles in a simulation.

**DETERMINATION OF  
ABSORBED DOSE BY  
RADIOPHOTOLUMINESCENCE  
DOSIMETRY AND MONTE  
CARLO SIMULATIONS**

**Aleksi Saikkonen**





**TURUN  
YLIOPISTO**  
UNIVERSITY  
OF TURKU

# **DETERMINATION OF ABSORBED DOSE BY RADIOPHOTOLUMINESCENCE DOSIMETRY AND MONTE CARLO SIMULATIONS**

---

Aleksi Saikkonen

## University of Turku

---

Faculty of Science  
Department of Physics and Astronomy  
Physics  
Doctoral Programme in Exact Sciences (EXACTUS)

### Supervised by

---

Adjunct Professor Jani Keyriläinen  
Department of Medical Physics  
Turku University Hospital  
Turku, Finland

Adjunct Professor Jarkko Ojala  
Department of Medical Physics  
Tampere University Hospital  
Tampere, Finland

### Reviewed by

---

Professor Miika Nieminen  
Research Unit of Health Sciences and  
Technology  
University of Oulu  
Oulu, Finland

Assistant Professor Tomislav Bokulic  
Department of Physics  
Faculty of Science  
University of Zagreb  
Zagreb, Croatia

### Opponent

---

Adjunct Professor Paula Toroi  
Principal Advisor  
The Radiation and Nuclear Safety  
Authority  
Vantaa, Finland

The originality of this publication has been checked in accordance with the University of Turku quality assurance system using the Turnitin Originality Check service.

Cover Image: Aleksii Saikkonen

ISBN 978-951-29-9209-6 (PRINT)  
ISBN 978-951-29-9210-2 (PDF)  
ISSN 0082-7002 (Print)  
ISSN 2343-3175 (Online )  
Painosalama, Turku, Finland 2023

*"Never walk away from home ahead of your axe and sword. You can't feel a battle  
in your bones or foresee a fight."*

***-The Hávamál***

*"Life is a fight for territory and once you stop fighting for what you want, what you  
don't want will automatically take over."*

***-Les Brown***

UNIVERSITY OF TURKU

Faculty of Science

Department of Physics and Astronomy

Physics

ALEKSI SAIKKONEN: Determination of absorbed dose by radiophotoluminescence dosimetry and Monte Carlo simulations

Doctoral Dissertation, 86 pp.

Doctoral Programme in Exact Sciences (EXACTUS)

April 2023

## ABSTRACT

Radiation therapy (RT) utilizes the harmfulness of ionizing radiation for good, with the goal of destroying cancer cells without damaging too much healthy tissue. Dosimetry is always needed to achieve this goal. Dosimetry is a branch of physics the purpose of which is to quantify the amount of radiation energy absorbed by a mass, i.e., a dose. Dose measurement has always been the basis of safe RT, and knowledge of the properties of dosimeters used is essential to obtain the most accurate results. Radiophotoluminescence dosimeters (RPLD) made of phosphate glass use the luminescence phenomenon to quantify the absorbed dose. Monte Carlo (MC) simulations, the gold standard for dose calculation, has been used in dosimetry research for a long time. By combining these two methods, flexible and accurate measurements with calculated theoretical values providing valuable information for research can be obtained.

The aim of this thesis was to investigate the use of radiophotoluminescence (RPL) dosimetry with MC simulations for verification of the planned absorbed dose in different geometries and radiation treatment modalities and beam qualities. Each part of this thesis had two objectives, the first of which was to investigate the irradiation system, the treatment modality, or both, and the second of which was to investigate dosimeters and calculation. The measurements used different dosimetric methods to compare the results with RPLDs and/or MC simulations.

The results suggest that RPLDs are versatile and rather easy-to-use dosimeters that are suitable for many different purposes. Their small size and energy response must be taken into account when planning measurements. The accuracy of MC simulations is widely known, although the results can only be as accurate as the model used. When creating a phantom, even with extra care a perfect model cannot be achieved due to the random nature of the materials. Both methods, RPL dosimetry and MC simulations, have their strengths and weaknesses, but together they complement each other. The theme of the thesis can be considered timely; the results will contribute to a better understanding of the advantages and limitations of the dosimetry methods currently used and assist in the development of clinical RT treatments.

**KEYWORDS:** radiation therapy, dosimetry, radiophotoluminescence dosimeter, Monte Carlo simulations, absorbed dose

TURUN YLIOPISTO

Matemaattis-luonnontieteellinen tiedekunta

Fysiikan ja tahtitieteen laitos

Fysiikka

ALEKSI SAIKKONEN: Absorboituneen annoksen määrittäminen

radiofotoluminesenssidosimetriaa ja Monte Carlo -simulaatioita käyttäen.

Väitöskirja, 86 s.

Eksaktien tieteiden tohtoriohjelma (EXACTUS)

Huhtikuu 2023

## TIIVISTELMÄ

Sädehoito on kirurgian ja lääkehoidon ohella syöpäsairauksien perushoitomuoto, jonka vaikutus perustuu toisaalta syöpäsolujen sädeherkkyyteen ja toisaalta normaalikudoksen kykyyn toipua sädetyksestä. Sädehoidon onnistumisen edellytyksenä on se, että määrätty annos on oikean suuruinen ja että se saadaan kohdennettua halutulle alueelle siten, etteivät kriittiset elimet tai kudokset saa niille asetettuja toleranssirajoja suurempia annoksia. Tämän tavoitteen saavuttamiseen tarvitaan dosimetriaa, fysiikan osa-alueita, jonka tarkoituksena on määrittää absorboituneen säteilyn energiamäärä massayksikköä kohden, eli absorboitunut annos. Annosmittaukset ovat aina olleet turvallisen sädehoidon perusta, ja dosimetrien eli annosmittarien tunteminen mahdollistaa tarkkojen tuloksien saavuttamiseen. Radiofotoluminesenssidosimetrit (RPLD) ovat fosfaattilasista valmistettuja annosmittareita, jotka hyödyntävät annoksen tallentamiseen luminesenssi-ilmiötä. Monte Carlo (MC) –simulointia voidaan sanoa annoslaskennan kultaiseksi standardiksi ja sitä on käytetty jo kauan annosmittaustutkimuksissa. Yhdistämällä nämä kaksi tapaa, monimuotoinen ja tarkka annosmittaus ja teoreettinen annoslaskenta, on tutkimuksen kannalta tärkeä tieto tällöin saavutettavissa.

Väitöskirjan tavoitteena oli tutkia radiofotoluminesenssi (RPL) -dosimetriaa ja MC-simulaatioita suunnitellun annoksen varmistamiseksi, kun käytössä on eri sädetyksgeometrioita ja -energioita. Jokaisella osatyöllä on kaksi tarkoitusta, joista ensimmäinen on kyseisen säteilylaitteen, hoitomuodon tai molempien tutkiminen ja toinen on annosmittausten ja -laskennan tutkiminen. Mittauksissa käytettiin useita eri annosmittausmenetelmiä, joilla saavutettuja tuloksia verrattiin RPLD-mittausten ja MC-simulointien tuottamiin tuloksiin.

Tutkimustulokset osoittavat RPLD:ien olevan monipuolisia ja suhteellisen helppokäyttöisiä annosmittareita, jotka soveltuvat useisiin eri käyttötarkoituksiin. Niiden pieni koko, suuntariippuvuus ja energiavaste tulee kuitenkin huomioida huolellisesti mittausten suunnittelussa. MC-simulointi on tarkkuudestaan tunnettu menetelmä, mutta on hyvä tiedostaa, että laskennalla saatavien tulosten tarkkuus vastaa käytettyjen mallien tarkkuutta. Mallien ja fantomien valmistamisessa täytyy muistaa, vaikka noudattaisikin erityistä huolellisuutta, että materiaalin satunnaisen rakenteen takia ei täysin täydellistä mallia pystytä koskaan luomaan. Molemmilla menetelmillä, RPL-dosimetria ja MC-simulointi, on omat vahvuutensa ja heikkoutensa, mutta yhdessä käytettynä ne täydentävät hyvin toisiaan. Väitöskirjan tutkimusaihetta voidaan pitää ajankohtaisena, ja tutkimustulokset ovat suoraan hyödynnettävissä kliinisen sädehoidon kehitystyössä.

ASIASANAT: sädehoito, dosimetria, radiofotoluminesenssiannosmittari, Monte Carlo -simulointi, absorboitunut annos

# Acknowledgements

Life is a long journey, with multiple objectives or stops on the way. One might say it's fractioned. Well, one fraction has now been completed to and it's time to think about how I got here. A young man with a good memory and a knack for aping, didn't know what to do, and went to the University of Turku. At some point during that trip, he heard about the profession of a medical physicist, which began to steer the trip in a certain direction. And here I am, doing things that come naturally to me, helping others, playing with machines, learning new things and being a physicist. Now is not the time to ride a motorcycle into the sunset singing "Rock Hard Ride Free", but to point the nose towards new challenges.

If I started writing a thank you to all the people who helped me, it would be a book of its own. For now, however, these couple of pages will have to be enough. First and foremost, I would like to thank my supervisors, Jani Keyriläinen and Jarkko Ojala, who have guided and shared their immeasurable wisdom to the young scientist. Jani, who in his endless patience, has developed projects for me that require thinking outside the box. And Jarkko, who has always helped me strive for even more accurate Monte Carlo simulations. It has been a great privilege to work with you and I hope that our collaboration will continue after this dissertation.

I wish to thank the reviewers, Professor Miika Nieminen and Assistant Professor Tomislav Bokulic, for giving their valuable time and effort to review this thesis. And also (perhaps a little too hastily) my opponent Adjunct Professor Paula Toroi, who will help/helped me to finalize this process. Not forgetting the custos, Professor Jarno Salonen, who showed in his lectures that things can be taught with humor.

Next, I would like to thank my co-authors, Jarkko Niemelä, Petri Sipilä and Eeva Boman, for their help and wisdom with the publications. Now is a good time to also give thanks for Professor Mika Teräs, Chief Physicist at Turku University Hospital, who generously gave me guidance, opportunities, and temporary positions during the internship. Without leaving out my other colleagues, physicists, co-workers, buddies, etc. from TYKS and Satasairaala, who have helped me on this journey. You managed to make work feel like a hobby. Especially for Radiotherapy Department, where only good ideas flew in the air during dose optimizations.

Special thanks to my fellow students from university for helping the time pass faster. To a few of those who always made me try harder with just a few insults. And thanks to old friends, a small unit/party in a fictional pub, who have taken it their mission to try to laugh at my old, plagiarized jokes.

I dedicate this last chapter to my family. Thanks to my parents who both helped me in their own way. And thanks to my horde of siblings for keeping my feet on the ground. Not forgetting the relatives who tried to look interested when I answered their question "how are your studies going?", thank you. And, finally, thanks to my beloved Satu and her patience with my stubbornness. Oh, how time flies, still much to do, "Aika rientää ja housut kuluu.", "Peace Out" \*drop the mic\*.

February 23, 2023  
*Aleksi Saikkonen*

# Table of Contents

<b>Acknowledgements</b> .....	<b>6</b>
<b>Abbreviations</b> .....	<b>9</b>
<b>List of Original Publications</b> .....	<b>10</b>
<b>1 Introduction</b> .....	<b>11</b>
<b>2 Theory</b> .....	<b>13</b>
2.1 Absorbed dose.....	13
2.2 Radiophotoluminescence dosimetry.....	16
2.3 Monte Carlo simulations.....	19
2.3.1 External beam simulations .....	20
2.3.2 Internal source simulations.....	26
2.4 Other methods .....	29
<b>3 Aim of the Thesis</b> .....	<b>31</b>
<b>4 Materials and Methods</b> .....	<b>32</b>
4.1 Cell and small animal x-ray irradiation system.....	32
4.1.1 Measurements with an x-ray irradiation system.....	32
4.2 Total body x-ray irradiation.....	33
4.2.1 Measurements for total body x-ray irradiation.....	33
4.2.2 Simulations for total body x-ray irradiation.....	34
4.3 Keloid scar gamma ray irradiation .....	35
4.3.1 Measurements for keloid scar gamma ray irradiation ..	35
4.3.2 Simulations for keloid scar gamma ray irradiation .....	36
<b>5 Summary of the Results (I-III)</b> .....	<b>39</b>
<b>6 Discussion</b> .....	<b>40</b>
<b>7 Conclusions</b> .....	<b>43</b>
<b>List of References</b> .....	<b>45</b>
<b>Original Publications</b> .....	<b>51</b>

# Abbreviations

AAA	analytical anisotropic algorithm
AAPM	American Association of Physicists in Medicine
BP2	Blue Phantom 2
BT	brachytherapy
CA	collimator angle
CAX	central axis
CM	component module
CT	computed tomography
ECUT	electron cutoff energy
GUI	graphical user interface
HDR	high dose rate
IC	ionization chamber
LDR	low dose rate
linac	linear accelerator
MC	Monte Carlo
MLC	multi-leaf collimator
MORTRAN	more formula translation
MU	monitor unit
PC	polycarbonate
PCUT	photon cutoff energy
PDD	percentage depth dose
phsp	phase space
PMMA	polymethyl methacrylate
RPL	radiophotoluminescence
RPLD	radiophotoluminescence dosimeter
RT	radiation therapy
SSD	source-to-surface distance
TBI	total body irradiation
TG-43	Task Group No. 43
TLD	thermoluminescence dosimeter
TPS	treatment planning system

# List of Original Publications

This dissertation is based on the following original publications, which are referred to in the text by their Roman numerals:

- I Saikkonen A, Niemelä J, Sipilä P, Keyriläinen J. Commissioning of the MultiRad 350 cell and small animal x-ray irradiation system. *Physica Medica*, 2019; 59: 107-111.
- II Saikkonen A, Ojala J, Keyriläinen J. Analytical anisotropic algorithm calculation in total body irradiation: a comparison with Monte Carlo calculation and dosimetry. *Journal of Cancer Science and Clinical Therapeutics*, 2021; 5: 458-473.
- III Saikkonen A, Ojala J, Sipilä P, Boman E, Keyriläinen J. Validation of the high-dose-rate brachytherapy doses in keloid scar treatment using the egs\_brachy Monte Carlo code. *Physics in Medicine & Biology*, accepted 2023.

The original publications have been reproduced with the permission of the copyright holders.

# 1 Introduction

A seemingly mysterious phenomenon called radiation is all around us, occurring both in nature and artificially. Its detrimental effects have been widely studied, and much is yet to be understood. Although the harmfulness of ionizing radiation is well known, this dangerous feature can also be used for good, such as in radiation therapy (RT). The goal of RT is to destroy cancer cells without damaging too much healthy tissue, but this cannot be achieved without proper dosimetry of the ionizing radiation. Dosimetry is a field of physics aimed at quantifying the amount of radiation energy absorbed by a mass, i.e. an absorbed dose.

Absorbed dose measurement has always been the foundation of safe RT, and knowledge of the tools used, i.e. dosimeters, is essential to obtain the most accurate results [1]. The properties of dosimeters have long been studied and their use is well documented by professional societies such as the American Association of Physicists in Medicine (AAPM) [2]. Knowledge of dosimeters means that the user knows how they work in different environments or scenarios, and to what extent quantities such as air pressure and temperature affect the results. Different qualities of the radiation beam can also have a sizeable impact, and special care must be taken when dealing with non-monoenergetic radiation. The distance between the measurement point and the radiation source can also alter the outcome. All of these must be considered when aiming for the most accurate results. That said, the accuracy should be sufficient for drawing conclusions and it is not always worth aiming for the extremes.

Radiophotoluminescence (RPL) is a luminescence effect observed in some minerals or types of glass following exposure to ionizing radiation. This phenomenon is exploited in dosimetry using a radiophotoluminescence dosimeter (RPLD), which can be shaped into small glass rods with a plastic cover for protection. The RPLD can be used to monitor radiation doses for environmental, personal, or research purposes [3]. Its advantages include multiple readout times, small size, flexible use, very low readout fading, and a wide measurable dose range.

Monte Carlo (MC) simulations are considered the gold standard for dose calculation. They have been used for decades in dosimeter research thanks to the accuracy and flexibility of different codes, such as EGSnrc and Geant4. It can be used e.g., for determining ionization chamber (IC) correction factors [4] or designing

new ICs [5]. It is also used to develop fast calculation algorithms for clinical RT treatment planning [6]. In research, the results of MC simulations can be used as theoretical values, providing a valuable perspective especially when combined with dose measurements. Clinical treatment planning algorithms calculate doses and dose distributions, while MC simulates particle interactions: dose is only one outcome.

This thesis investigates the use of RPLDs with MC simulations. After a brief introduction in Chapter 1, the main topic of the thesis is discussed in Chapter 2. It consists of absorbed dose, RPL dosimetry, MC simulations, and a brief overview of other methods used. Chapter 3 summarizes the aims of the thesis and Chapter 4 describes the study-specific materials and methods. The results are summarized in Chapter 5 and discussed in Chapter 6, and the conclusions are presented in Chapter 7.

## 2 Theory

### 2.1 Absorbed dose

Electromagnetic waves form the electromagnetic spectrum, which has a range of portions categorized by either wavelength, energy, or frequency. The best known of these is visible light, which has a wavelength range of 380–750 nm. The rest of the spectrum is invisible to the human eye. The two portions with the shortest wavelength, x-rays and gamma rays, are classified as ionizing radiation [7].

When ionizing radiation passes through a material, the kinetic energy of the particles (photons, electrons, etc.) is absorbed through interactions with the molecules and atoms, creating secondary particles and energy transfer to the material. The average energy transferred to the material ( $d\bar{\epsilon}$ ) is obtained by calculating the difference between the energy of the radiation incident on volume  $V$  having mass  $m$  into the material ( $R_{in}$ ) and the energy of the radiation emerging from the material ( $R_{out}$ ) [8]

$$d\bar{\epsilon} = R_{in} - R_{out} + \sum Q, \quad (1)$$

where  $\sum Q$  is the change in rest energy. The absorbed dose ( $D$ ) is the amount of average energy ( $d\bar{\epsilon}$ ) absorbed per unit mass ( $dm$ ) [8]

$$D = \frac{d\bar{\epsilon}}{dm}. \quad (2)$$

The unit of absorbed dose, J/kg, is the gray (Gy) [8]. The absorbed dose is an internationally agreed prescription quantity in RT and is measured in a known material such as water. This is usually the case in RT dose measurements [9]. In measurements, the dose can also be measured in a water-mimicking material such as solid water [10].

The IC is one of the most widely used detectors for measuring absorbed dose [11]–[13]. An IC is usually a gas-filled detector where the gas is contained in a chamber with two electrodes (Figure 1). Upon impingement by ionizing radiation into the chamber, ion pairs are created in the gas and attracted to the electrodes,

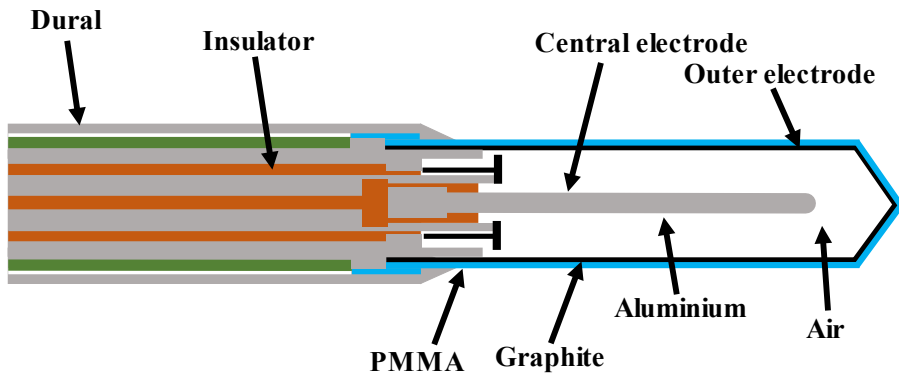


**Figure 1.** Illustration of a Farmer-type gas-filled ionization chamber (modified from [13]).

between which a voltage potential has been created to form an electric field. As the electrodes collect the ion pairs, the resulting ionization current between them can be measured with an electrometer. If all the ion pairs are collected, the current is directly proportional to the absorbed dose in the chamber. An IC can use different gases such as air, argon, or various gas mixtures [14]. Most ICs used in measurements are air-filled ambient pressure chambers or vented chambers with a small channel or vent to equilibrate the IC to the atmosphere [14], [15].

To get the most accurate results, correction factors are used with ICs. These factors are usually calculated using MC simulations, which are discussed in more detail in Chapter 2.3, and which take into account many physical properties of the IC [16]. In this thesis, absorbed dose measurements fall into two energy-based categories, high- and low-energy radiation. High-energy radiation has more penetrating power than low-energy radiation, which has a bearing on the correction factors used.

High-energy radiation, such as a 6 MV x-ray (photon) beam, is used in clinical external beam RT, where absorbed dose measurements are well standardized [17]. Measurements are usually performed following a dosimetry protocol based on absorbed dose to water. Reference conditions such as distance to the radiation source, water depth, and field size are considered in the protocol to make the results comparable. The absorbed dose to water ( $D_{w,Q}$ ) with a beam of quality  $Q$  can be calculated as follows [17]:

$$D_{w,Q} = M_Q N_{D,w,Q_0} k_{Q,Q_0} , \quad (3)$$

where  $M_Q$  is the current measured from the IC,  $N_{D,w,Q_0}$  is the calibration factor of the absorbed dose in water, and  $Q_0$  is the beam quality used in the calibration of the IC.  $k_{Q,Q_0}$  is the correction factor for the difference between the calibration beam quality  $Q_0$  and the used beam quality  $Q$  [17]. If  $N_{D,w,Q_0}$  takes into account the difference between the beam qualities ( $k_{Q,Q_0}$ ) and more measurement-specific correction factors are applied, Equation 3 takes the form [1]

$$D_{w,Q} = M N_{D,w,Q} k_{Tp} k_s k_{pol} k_{elec} , \quad (4)$$

where  $k_{Tp}$  is the temperature and pressure correction factor,  $k_s$  is recombination correction factor,  $k_{pol}$  is the polarity correction factor, and  $k_{elec}$  is the correction factor for electrometer [1].

Low and medium kilovoltage x-ray beams are usually used in diagnostic medical imaging, such as planar imaging or computed tomography (CT) [18]. They can also be used for irradiating cells or small animals. In this case, the energy can be a bit higher than in diagnostic imaging, or ‘medium-energy’. Absorbed dose measurements with IC, when low- or medium-energy irradiation (40-300 kV) is used, require different corrections than those with high energy. The absorbed dose in water ( $D_w$ ) can be calculated with two measurement methods, in-air or in-phantom. The following equation is used for the in-phantom method [19]:

$$D_w = M_L N_k P_{Q, cham} P_{sheath} [(\bar{\mu}_{en}/\rho)_{air}^w]_{water} , \quad (5)$$

where  $M_L$  is the electrometric reading from the IC including all the correction factors in Equation 4, and  $N_k$  is the air-kerma calibration factor.  $P_{Q, cham}$  is an overall IC correction factor that takes into account corrections for air cavity, walls, chamber stem, energy change, and photon beam angular distribution in the phantom compared with calibration.  $P_{sheath}$  is a correction factor for a waterproof sleeve.  $[(\bar{\mu}_{en}/\rho)_{air}^w]_{water}$  is the water-to-air ratio of the mean mass energy-absorption coefficients. The  $P_{sheath}$  factor is only used when a separate waterproof sleeve is attached to the IC [19]. ICs used in dose-in-water measurements are usually manufactured waterproof with a coating or other structural means, in which case this factor is not needed. These correction factors are tabulated in the AAPM Task Group No. 61 Report [19].

In this thesis, the IC was used to determine absorbed dose correction factors for RPLDs to obtain the most accurate results. The correction factor was calculated from measurements where the irradiation was repeated with the same parameters for both IC and RPLDs in a water phantom. Five or more RPLDs were used in the measurements and the correction factor was calculated as the ratio of absorbed doses.

## 2.2 Radiophotoluminescence dosimetry

Luminescence is a phenomenon whereby light is emitted from the excited electronic state of a molecule. In the photoluminescence of atomic species the emission wavelength is equal to the absorption wavelength, i.e. the excitation wavelength, but usually in the case of molecules the emission wavelength is longer. Photoluminescence can be observed in gas, liquid or solid phase [20]. RPL is a property observed in some minerals or glasses when the compound becomes luminescent after exposure to ionizing radiation [21]. Electrons in the material are excited by ultraviolet light and, when they return to their original state, fluorescence is emitted from the color centers. Electrons in the color center return to the electron trap after emission [3].

The RPLD uses the RPL effect to register absorbed doses. These dosimeters come in many shapes and are made of silver-activated phosphate glass. The dosimetric properties are based on the reaction of positive silver ions ( $\text{Ag}^+$ ) and phosphate ions ( $\text{PO}_4^-$ ) in the glass. When exposed to radiation,  $\text{PO}_4^-$  loses one electron and forms a hole ( $\text{hPO}_4$ ). The reaction has two options: either the loose electron combines with  $\text{Ag}^+$  and is reduced to  $\text{Ag}^0$ , or  $\text{hPO}_4$  causes oxidation and combines with  $\text{Ag}^+$  to form  $\text{Ag}^{2+}$ .  $\text{Ag}^0$  and  $\text{Ag}^{2+}$  are color centers, namely RPL centers, which are stable energy states [22].

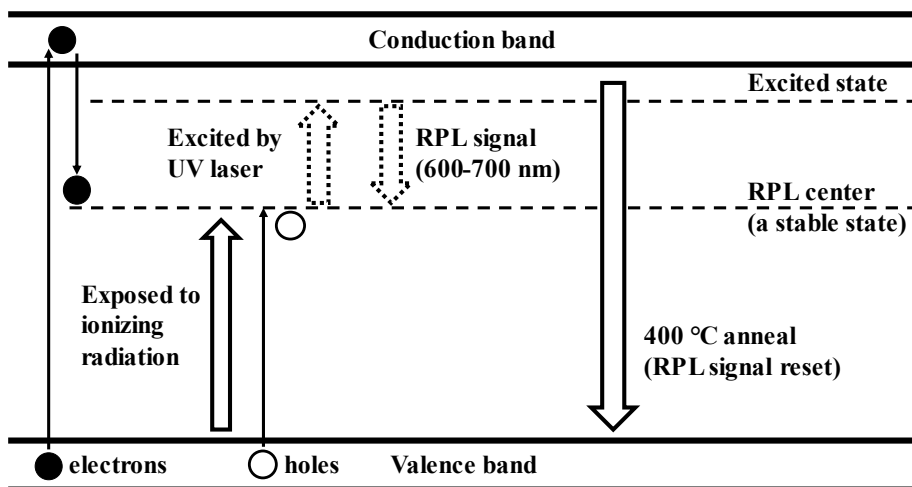
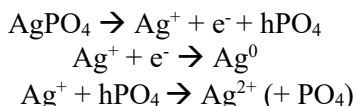


**Figure 2.** Radiophotoluminescence dosimeter (RPLD) energy band map. After exposure to ionizing radiation,  $\text{Ag}^+$  combines with an electron or  $\text{hPO}_4$  to form a radiophotoluminescence (RPL) center (stable state). The centers are excited by ultraviolet light and emit orange light when returning. RPLDs are annealed in hour-long heating at 400 °C (modified from [25]).



When an ultraviolet beam (337.1 nm) produced by the N<sub>2</sub>-laser pulse is applied to the RPL centers, they are excited. As the electrons return to the stable state, a photon emission of orange light wavelength (590–630 nm) occurs. The number of RPL centers remains constant after the emission, which gives RPLDs their inherent re-reading ability. The number of photons emitted is proportional to the number of RPL centers, both of which are proportional to the absorbed energy and absorbed dose [23]. To release electrons from RPL centers, they need much higher energy, which can be achieved with heat. When dosimeters are heated to 400 °C for an hour, the chemical process is reversed and the glass returns to its original empty state [24]. The behavior of the RPLD and its energy states throughout the process are presented in Figure 2 [25].

Dose Ace GD-302M and GD-352M RPLDs (AGC Techno Glass Co., Shizuoka, Japan) are designed for dose measurements and contain different elements (Figure 3). Their atomic weight composition is 31.55 % P, 51.16 % O, 6.12 % Al, 11.00 % Na, and 0.17 % Ag. The dosimeters are cylindrical in shape and have a diameter of 1.5 mm and length 12.0 mm. Their effective atomic number is 12.04 and the density is 2.61 g/cm<sup>3</sup> [26]. There is no difference between the glass rods of the GD-302M

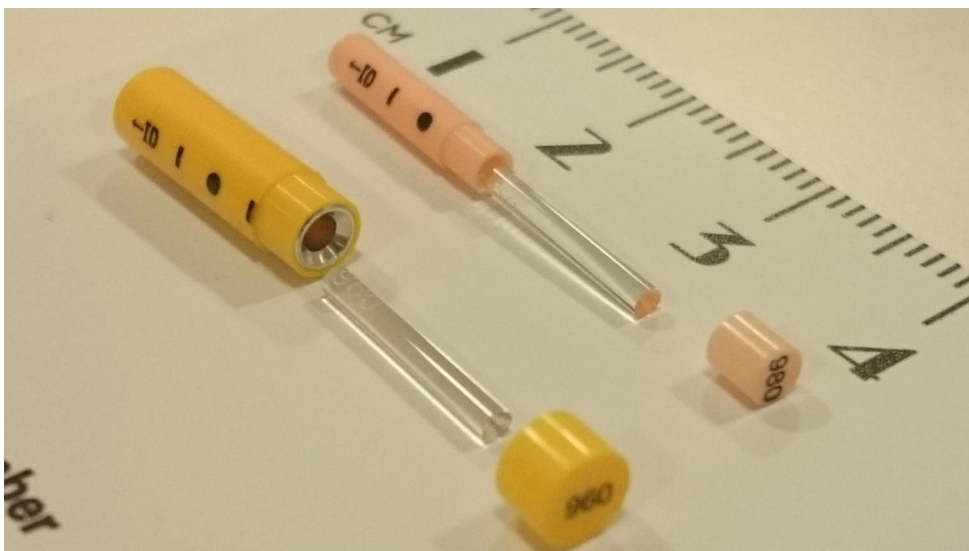


**Figure 3.** Dose Ace GD-302M (light red) and GD-352M (yellow) dosimeters. Each dosimeter has its own identification number engraved on the end of the rod. The size difference is due to the Sn filter in the yellow shell.

and GD-352M types. The difference is in the polymethyl methacrylate (PMMA) shell that covers the glass. The GD-352M has a Sn filter embedded in a PMMA shell, making it larger than the GD-302M shell, measuring  $4.3 \times 14.5 \text{ mm}^2$  compared with  $2.8 \times 13 \text{ mm}^2$ , respectively [27]. The Sn filter is designed to stop low energy photons from offsetting the energy dependence of RPLDs [28]. Figure 4 shows the energy dependence curves of GD-series RPLDs and thermoluminescence dosimeters (TLD) for comparison [3]. The energy dependence of RPLDs has been extensively studied over a wide energy range (30 keV–100 GeV) [25], [29], [30].

The manufacturer has classified that both RPLDs can be used in the standard dose range (from  $10 \text{ }\mu\text{Gy}$  to 10 Gy) and the GD-302M also in the high-dose range (1–100 Gy). In addition, the GD-302M must be used with energy above 120 keV [27]. These features make the GD-302M ideal for measuring doses used in RT and the GD-352M for measuring doses used in diagnostic imaging. When using GD-352M RPLDs, the strong angular dependence of the dosimeter on its long axis must also be taken into account [31]. RPLDs made of undoped LiF can be used to measure very high doses (1–15 kGy). What makes this special is that LiF is usually used as a TLD material [32].

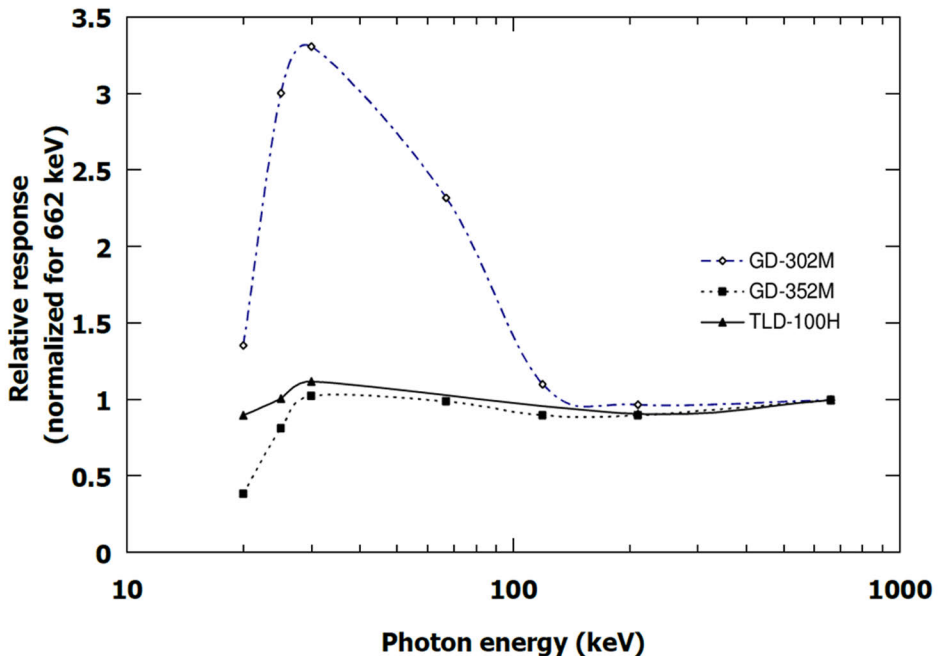


**Figure 4.** Illustration of the energy dependence curves of radiophotoluminescence dosimeters (GD-302M, GD-352M) and thermoluminescence dosimeter (TLD-100H) (modified from [3]).

In this thesis, RPLDs were pre-heated at 70 °C for 30 min before reading, then allowed to cool to room temperature. This is done to accelerate build-up during which the amount of RPL fluorescence in the glass element increases and stabilizes [27], [33]. Dosimeter reading was done with the Glass Dosimetry Reader FGD-1000 (Dose Ace, AGC Techno Glass Co., Shizuoka, Japan), which has two types of magazines, standard and high-dose, for reading the dose. The standard magazine is for doses below 10 Gy and the high-dose magazine for doses of 10 Gy to 500 Gy [33]. The reader has one calibration per magazine: against 6 mGy with a Cs-137 source for the standard magazine and  $(2 \pm 0.5)$  Gy with a Cs-137 source for the high-dose magazine. Both calibrations are performed in air. The user can change the calibration based on his/her own measurements. For example, when calibrating the standard magazine, the user selects a calibration mode for reading the RPLD irradiated with a known dose (e.g., manufacturer's 6 mGy with a Cs-137 source). After the reading, the user has the option to enter the correct RPLD dose and the program calculates the correction factor using the read value and the correct value. In this thesis, the calibration of the reader was not changed.

To ensure that doses measured by the RPLD are accurate, calibration must be performed using known calibrated dosimetry (e.g., IC, TLD, etc.) [23], [26], [34]. Typically, the calibration is based on IC measurements under reference conditions at beam quality  $Q$ , where exactly the same dose is irradiated into both the IC and RPLD [23]. When the correction factor is calculated from the ratio of the calculated IC doses (Equation 3) and the RPLD doses read by the reader, the accuracy depends more on the other characteristics of the RPLD and the measurement setup. Characteristics such as dose linearity, energy dependence, angular dependence, fading effect and reproducibility have been widely studied and their effect can be reduced with good measurement procedures [23], [31], [35]. In this thesis, the setting of the calibration measurements were adjusted as close as possible to the irradiation settings of the respective measurement (i.e., radiation energy, distance from source, medium, dose, dose-rate, etc.). The RPLDs were always oriented with the long side towards the radiation beam/source and the readout was performed after pre-heating within 12 hours of irradiation. With this procedure, the greatest source of error probably lies in the measurements and other, unpredictable, causes. Calibration of used ICs is performed every 3 years in a secondary standard dosimetry laboratory.

## 2.3 Monte Carlo simulations

MC simulations, methods, calculations, or experiments are a group of computational algorithms that use repeated random sampling to obtain numerical results. MC simulations can be used to resolve macroscopic problems based on the interactions of microscopic particles like photons, electrons, neutrons, and atoms. MC

simulations gain superiority as the simulated problems become more complex [36]. In MC simulations, particle interactions are simulated using probability distributions. The interactions create tracks and trajectories for the particles, called particle histories. The particle history also includes all secondary particles created in the interaction. At the end of the simulations, the results can be seen as the average of particle histories [37]. The simulation commands are given in an input file that describes all the detailed information needed to perform the simulation, e.g., settings, modeled structures with materials, and regions of interest or scoring volumes. In this thesis, MC simulations were performed with the EGSnrc (Electron Gamma Shower, National Research Council, Ottawa, ON, Canada) software toolkit [38].

The goal of making an MC model for simulations is to model as accurately as possible everything between the source and the phantom that can affect the dose. In the model, the volume where the dose is calculated is called the scoring volume. Scoring means counting the average particle histories, i.e., the interactions in a defined volume, which can be used to calculate either the relative or absolute absorbed dose [36]. These particle histories can be seen as a point in  $d$ -dimensional space, where  $d$  represents the number of interactions. In this case, taking the history average is equivalent to  $d$ -dimensional MC integration. This introduces statistical uncertainty into the simulations, which depends on the number of histories. Statistical uncertainty usually decreases by a factor of two if the number of histories increases by a factor of four [39]. In some cases, the scoring object can be used as a source for the subsequent simulation [40]. The object is then called a phase space file (phsp file). The phsp file contains complete information about the particle history. This may include e.g., particle direction, energy, type, position, statistical weight, and interactions before this point [41].

In this thesis, MC simulations were used to calculate the theoretical values of absorbed doses in order to compare them with RPLD results. The statistical uncertainty aimed for in the simulations was 0.5 % or less. The comparison was also performed for each measurement of Studies **II** and **III**.

### 2.3.1 External beam simulations

The most commonly used treatment unit in external beam RT is a medical linear accelerator (linac) (Figure 5). A linac produces electrons with an electron gun and uses linear accelerating waveguides to give them up to 20–25 MeV of energy. These electrons then collide with a target to produce an x-ray (bremsstrahlung) beam or with a scattering foil to produce a broad electron beam. The produced electron beam is first focused, steered, and bent with magnets, then fed into the linac head in which

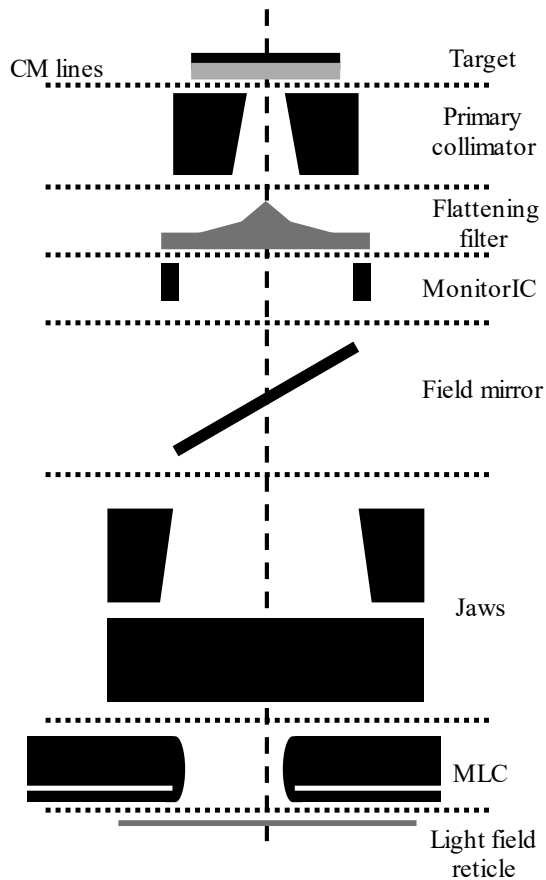


**Figure 5.** Schematic drawing of the linear accelerator model. Component modules (CM) lines separate different modules used in the BEAMnrc software (IC: ionization chamber, MLC: multi-leaf collimator) (modified from [36]).

either a broad electron beam can be produced with a scattering foil and further shaped with applicators, or photons are produced in the target and then the beam shaping depends on the magnets and the primary collimator, and finally with secondary collimators (jaws) and multi-leaf collimators (MLC) for accurate treatment delivery [9]. Linacs are designed for RT treatments and are often capable of producing photon and electron beams with different nominal accelerating potentials. They can be equipped with e.g., 6 MV, 10 MV, 15 MV, and 18 MV photon energies, as well as 6 MV and 10 MV flattening filter-free energies [42], [43].

MC simulations of the external beam RT can be performed using a combination of two applications from the EGSnrc software toolkit: BEAMnrc and DOSXYZnrc

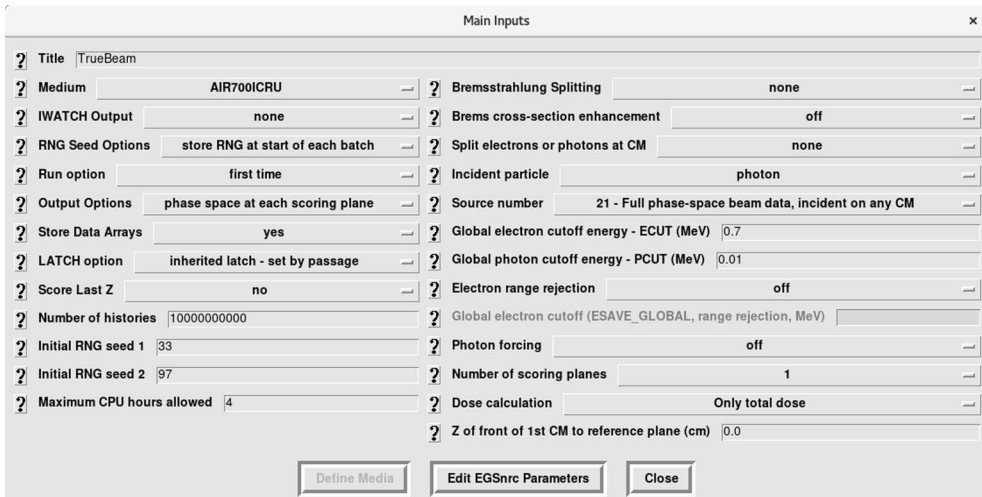


**Figure 6.** Example of the main input parameter window in BEAMnrc. The help button (?) is on the left of each input.

[44], [45]. Both applications use MORTRAN (more formula translation) code and can be accessed via either an input file or a graphical user interface (GUI).

The BEAMnrc application, an EGSnrc implementation of the BEAM code, is one of the most used and cited codes for linac modeling because of its easy-to-use building block approach [36]. The BEAMnrc GUI is made to facilitate the input file [46]. In the GUI, each input has its own help button that describes the input and its options. The BEAMnrc GUI is divided into two parts: main input parameters and geometries, i.e. component modules (CM).

The main input parameter window (Figure 6) contains all the parameters required for the simulation that are not related to individual geometries. These parameters include e.g., number of histories, global cutoff energies, both source and output options, and many different interaction controls.

Global cutoff energies are divided into two parameters: photon cutoff energy ( $PCUT$ ) and electron cutoff energy ( $ECUT$ ). Both parameters define the minimum total energy below which the particle history is terminated, and the energy is deposited in the current region. The unit of value is MeV. The values recommended by the developers are  $ECUT = 0.521$  or  $0.700$  MeV and  $PCUT = 0.01$  MeV. These values depend on the type of simulation problem under consideration, and the choice is a compromise between the required accuracy and speed. Lower  $PCUT$  values can also be used without large penalties on the simulation time [47].

Source parameter controls are used for the radiation source. BEAMnrc has 13 different source types, each built for different cases. For example, there are a couple of different shapes of sources, such as a point source ( $ISOURC = 13$ ) or a cylindrical

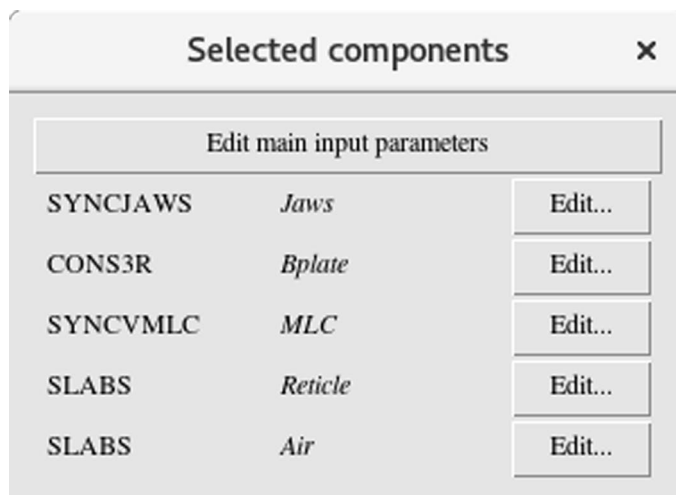


**Figure 7.** Example of the component module (CM) window in BEAMnrc.

source ( $ISOURC = 3$ ). There is also an option to use the phsp file source mentioned above ( $ISOURC = 21$ ) [47]. This option can simplify modeling, because the source can be stored after any CM and used in other simulations to replace all CMs above it. In Study II, this option was used as a source for the simulations. Phsp files were generated by the manufacturer of the treatment unit used.

In BEAMnrc, the output options are either with the phsp file or without. Phsp files are created after each scoring plane, which the user is free to choose [46]. The EGSnrc simulation also has a lot of interaction controls to choose which interactions (i.e. Compton scattering, photoelectric effect, etc.) are considered in the simulations. These controls are included in every EGSnrc software and the implementations are clearly described in the manual [39].

Geometries, or CMs in BEAMnrc, are the building blocks of a linac. The CMs are designed as part of the linac and each one is a horizontal slab stacked on top of another (illustration in Figure 5). Each module communicates with the rest of the system and has a specific purpose. For instance, there are modules named SYNC, which can be synchronized with each other and with the moving parts of the linac, i.e., the angle of the gantry, collimator, etc. [47]. When the user configures a new linac in the GUI, they first select the desired CMs and their order (Figure 7), after which all the necessary parameters can be filled [46]. In this thesis, the focus is on the jaws, collimator baseplate, MLC, and light field reticle, as these CMs were used in Study II.

JAWS is a CM used for jaws. In linacs, the jaws are usually the upper secondary collimator and are used as the delimiter for treatment. There are two sets of jaws,

oriented in the X and Y directions, and they define a rectangular symmetrical area of the beam. The opening of the jaws is determined by four distances from the beam axis, two per jaw: upper and lower. There is also an option for the field type, from which one can choose a static, dynamic, or step-and-shoot field. The last two must contain a file with information about the fields. The GUI has a built-in feature that automatically calculates jaw opening using the field size at a given source-to-surface distance (SSD). An illustration of the JAWS module is shown in Figure 8 [47].

CONS3R is the CM used for the baseplate. The baseplate is a disk-shaped steel plate, the purpose of which stop the scattered radiation. The CONS3R module has two mediums, an outer and an inner, whose interface can be freely defined. An illustration of the CONS3R module is presented in Figure 8 [47].

There are many different CMs for MLCs, which are different types of commercially used MLCs. DYNVMLC CM was used in this thesis because it models MLCs in the used linac (Chapter 4.2) [47]. The MLC usually acts as the second secondary collimator and can be used as a beam shaper or intensity modulator [48]. The MLC consists of several leaves that can be controlled separately. The size and thickness of the leaves may vary depending on the model and supplier of the treatment unit [43], [49]. The DYNVMLC module has three different types of leaves: full, target and isocenter. All types have a unique shape and dimensions that must be carefully considered in the module parameters. As in the JAWS module, there is an option to change the field type. An illustration of the DYNVMLC module is presented in Figure 8 [47].

SLABS is the CM used for the reticle of the light field. The reticle can be used as an aiming aid for the RT. It is a plastic membrane, made of Mylar®, a type of stretched polyester film with two lines describing the axes. The SLABS module can consist of several slabs with different media. Only the thickness of the slabs is needed. An illustration of the SLABS module is presented in Figure 8 [47].

After building the CM and the entire linac model, there is a preview function to help visualize the module or model. The preview is a two-dimensional plane showing the model from the central axis (CAX). One can choose the direction from which the model is displayed (xz or yz view) [46].

DOSXYZnrc is code for simulating three-dimensional dose distributions in voxelized rectilinear phantoms. Just like BEAMnrc, DOSXYZnrc also has a GUI to simplify the process of creating an input file. The GUI has a single window from which all inputs can be controlled. The GUI also has a help button next to each input, like the BEAMnrc GUI [46].

DOSXYZnrc has two dedicated beam sources that can be used in many different configurations. The code also supports phsp sources and the full BEAMnrc model as a radiation source. The direction of the radiation beam can be controlled using the code, and several directions can be used in one simulation. For example, one can



combine BEAMnrc and DOSXYZnrc codes to calculate doses in phantom with multi-directional irradiation, where the jaws and MLC positions are synchronized with the beam direction, i.e., the gantry angle [45], [47].

DOSXYZnrc has two options for the phantom: self-defined or generated from CT data. When using a self-defined phantom, the user must specify the voxel dimensions and materials. This option can be used to model water phantoms. When CT data are used in phantom generation, DOSXYZnrc supports dose calculation for CT images. CT images can be converted using the *ctcreate* code, which converts the Hounsfield units of the images to a readable scale for DOSXYZnrc [45].

### 2.3.2 Internal source simulations

Internal RT or brachytherapy (BT) is an RT technique whereby the source is placed inside or near the treatment target [9]. BT treatment can be given with manual implantations or remotely with a treatment unit called an afterloader [50], [51]. There are several forms of BT, each for a different diagnosis—for example, intracavitary BT for gynecological, intraluminal for esophageal, and interstitial for breast cancer treatments [52]–[54]. Treatments are categorized as low dose rate (LDR), medium dose rate or high dose rate (HDR), the difference being the dose rate at the dose specification point. A remote controlled afterloader is most commonly used in HDR treatments. Afterloaders are self-shielded treatment units that, for safety reasons, transport the source remotely along applicators or catheters and can move the source to different stopping positions (dwells) during the treatment [9]. Modern afterloaders have many features that help make treatments safer and more accurate, such as quality assurance devices or electromagnetic tracking capability [55], [56].

In this thesis, the MC simulations of BT was performed using *egs\_brachy* code, which uses the *egs++* library of the EGSnrc software toolkit [57]. The *egs++* library is an EGSnrc code based on the C++ language, which gives it more flexibility in terms of geometry and source definitions. *egs++* comes with a viewer, *egs\_view*, which can be used to visualize geometries and particle tracks [58]. The *egs++* library is used by many EGSnrc applications, e.g. *egs\_chamber*, *egs\_cbct*, and *egs\_mird* [59]–[61].

*egs\_brachy* is used with input files, which present all the data for the simulations. The input file is divided into six main sections: run controls, geometry definitions, volume correction, source definition, scoring options, and MC transport parameters.

Run controls usually start a file and specify the number of histories used in the simulation (*ncase*). In the run control section, one can also specify how many portions or batch simulations are made (*nbatch*), the file format for *egsdat* files (*egsdat file format*), and how many geometry errors are allowed in the simulation

```

### Catheter
:start geometry:
  name = CAT
  library = egs_cones
  type = EGS_ConeStack
  axis = 14 0 0 -14 0 0
  :start layer:
    thickness = 28
    top radii = 0.07 0.1
    bottom radii = 0.07 0.1
    media = AIR_TG43 PMMA
  :stop layer:
:stop geometry:
:start geometry:
  name = air_box
  library = egs_box
  box size = 27 0.2 0.2
  :start media input:
    media = AIR_TG43
  :stop media input:
:stop geometry:
:start geometry:
  name = CAT_air
  library = egs_union
  geometries = CAT air_box
:stop geometry:

```

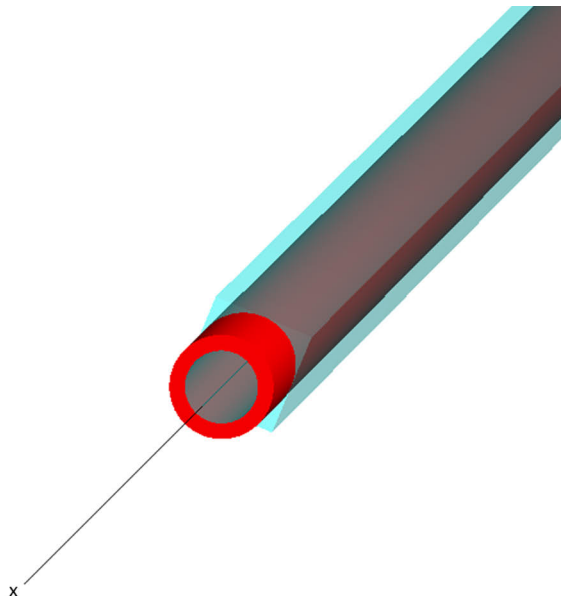


**Figure 9.** Geometry definition and illustration of the catheter geometry used in `egs_brachy` calculation. Illustration done with `egs_view` geometry viewer. Red is polymethyl methacrylate (PMMA) and light blue is air.

(*geometry error limit*). There is also the command, `nchunk`, which divides the simulation into chunks when several computers are used for parallel simulations. This makes it possible to balance the computing time if the computers have different calculation speeds [62].

The geometry definitions section defines all used geometries. The definition starts by selecting the geometry class i.e. the type or shape of the geometry (box, cylinder, sphere etc.), from the `egs++` library [58] and filling in all the necessary information to make the geometry (dimensions, rotations, materials, etc.). Geometries can then be arranged side by side or nested with another geometry class. Figure 9 shows an example of geometry definition and illustration of the catheter geometry. The geometry definition section must have definitions for the source (*source geometries*) and phantom (*phantom geometries*). The source geometries define which geometries are the actual source objects. The phantom geometries define scoring geometries for `egs_brachy`. The scoring geometry is limited to a sphere, cylinder, or cube. For source and phantom geometries, `egs_brachy` has its own library that can be used in simulations. The library contains many different sources, e.g. Ir-192 HDR source and I-125 LDR source and water phantoms [62].

The source definition section specifies information about the radioactivity of the source. The section defines the source charge (type of emitting particle), shape,

energy spectrum, and location. The charge defines the particles of radiation (photon, electron, or positron). The shape input defines the radioactive region within the source and is usually similar to the radioactive material of the source geometry. The energy spectrum can be either tabulated or monoenergetic, the first using an input file and the second an input key (*energy*) in MeV. The location input (*transformations*) defines the source coordinates, and there must be as many inputs as sources. If a moving source is used, one input can contain several coordinates [62]. *Source weights* can also be defined in the source definition, which is a list of the relative statistical weights of each source. This can be used to define different source activity levels or dwell times at stopping positions [63].

In the scoring options section, there are several different options for determining the type of scoring, i.e., recording the dose. Types, such as  $\bar{\mu}_{\text{en}}$  (*muen*), phsp file, or tracklength dose can be defined and used in simulations. Multiple scoring types can also be used. In this section, a dose scaling factor can be defined which gives the possibility to calculate the absorbed dose, for example to scale the results comparable to BT treatment or dose measurements [62]. The dose scaling factor ( $k_s$ ) can be calculated using the equation [62]

$$k_s = S_K^{\text{ref}} / S_K^{\text{hist}} \Delta t_{\text{max}}, \quad (6)$$

where  $S_K^{\text{ref}}$  is the air-kerma strength of the treatment source at the start of treatment,  $S_K^{\text{hist}}$  is the air-kerma strength per history of the simulation source, and  $\Delta t_{\text{max}}$  is the maximum individual dwell time, i.e. stopping time [62].

MC transport parameters is a section where all the simulation parameters necessary for transporting radiation are defined [62]. This section is similar to the BEAMnrc interaction controls (Compton scattering, photoelectric effect, bremsstrahlung, etc.). Changing the options (on, off, simple, etc.) can greatly affect the efficiency and accuracy of simulations, and each change should be carefully considered. The section also has inputs for transport cutoffs (*ECUT* and *PCUT*).

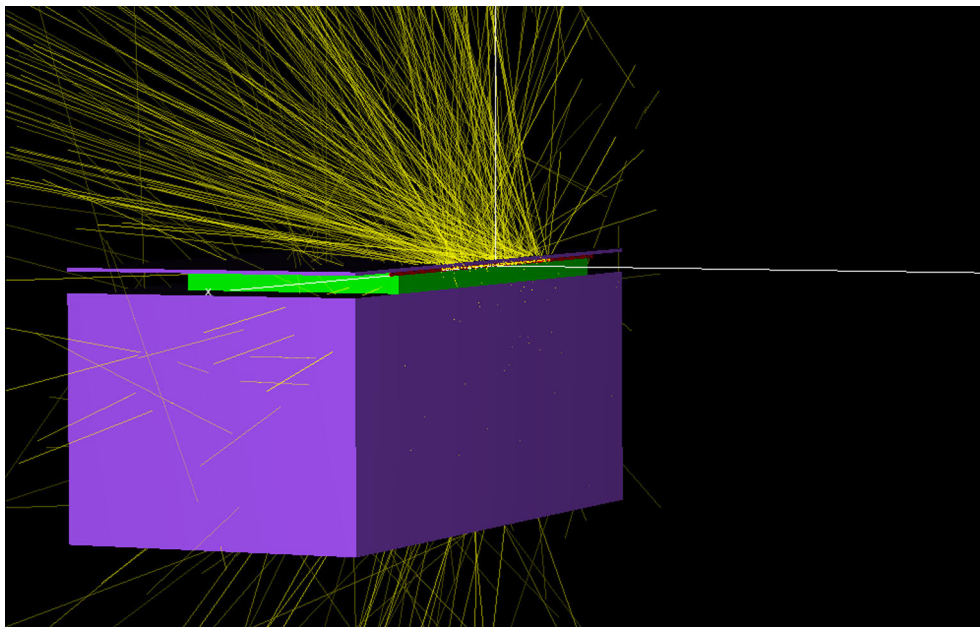


**Figure 10.** Modeled solid water phantom used in Study III with `egs_brachy`. The yellow lines represent tracked photons, the purple box is made of solid water, and the green slab is made of polycarbonate.

## 2.4 Other methods

In this thesis, a radiochromic film and two different calculation algorithms were used for comparison. This chapter describes them briefly.

The Gafchromic EBT3 (Ashland, Wayne, NJ, USA) radiochromic film is designed to measure the absorbed dose deposited by ionizing radiation. It is suited for high-energy photons and its dynamic range is applicable for a dose range of 0.2 to 20 Gy. EBT3 has a three-layer structure: two outer 125  $\mu\text{m}$  matte-polyester layers with an inner 28  $\mu\text{m}$  active layer in between. The color transform of the layers is proportional to the absorbed radiation dose and can be recognized with the naked eye [64]. The active layer consists of 56.8 % H, 27.6 % C, 13.3 % O, 1.6 % Al, and 0.6 % Li, and the effective atomic number of the film is 7.26 [65]. The use of radiochromic film is well documented by AAPM TG-235 (update to TG-55), and more information can be obtained from the report [66]. After irradiation, the films are scanned with a flatbed film scanner (e.g., Epson Perfection V700 Photo, Seiko Epson Corporation, Suwa, Japan) and the typical data format for images is Tagged Image File Format (TIFF). Images can be analyzed with analysis software (e.g. OmniPro - I'mRT, IBA Dosimetry GmbH, Schwarzenbruck, Germany).

Two different calculation algorithms were used: an anisotropic analytical algorithm (AAA, Varian Medical Systems Inc. (now merged with Siemens Healthineers), Palo Alto, CA, USA) and Acuros (Acuros BV, Varian Medical Systems Inc. (now merged with Siemens Healthineers)). Both algorithms are available in a commercial treatment planning system (TPS) and are widely used. AAA uses a convolution method with calculation terms for different photons and electrons, and Acuros uses a linear Boltzmann transport equation solver that describes the macroscopic behavior between particle interactions and matter in the calculation space [67], [68]. The main difference between the algorithms is the calculation medium and accuracy: AAA calculates the dose to water, while with Acuros the medium can be selected from a library. For this reason, Acuros is better in regions where the material properties differ substantially from water (bone, lungs, and interface regions) [6].

### 3 Aim of the Thesis

The aim of the thesis was to investigate the use of RPLDs in the verification of the planned absorbed dose obtained with different radiation modalities (different beam qualities for external beam irradiations and BT sources), and to compare it with MC simulations. This main aim was divided into specific aims presented in detail in the original publications (**I-III**):

**I.** To commission a commercial x-ray irradiation system to be used for cell and small animal studies. The study determined the characteristics of the irradiator and absorbed dose of the x-ray beam using relative and absolute dosimetry. This study observed the use of two different types of RPLD with kilovoltage x-rays. The research also served as a learning process for utilizing RPL dosimetry.

**II.** To investigate the feasibility and accuracy of a dose calculation algorithm in a commercial TPS for total body irradiation (TBI) with an extended SSD of 400 cm, comparing it with the dose calculated by MC simulations and the dose measured by different dosimetry methods. In this study, the effect of high-energy irradiations of RPLDs was observed. This study also introduced the MC simulations of this thesis and served as a springboard for the accurate modeling of the irradiation configuration such as the treatment unit, phantoms, and materials.

**III.** To investigate the feasibility and accuracy of the absorbed dose delivered by an HDR afterloader in keloid scar BT using dose measurements and MC simulations. The aim was also to compare HDR afterloaders from two different manufacturers and the accuracy of the common dose model.

## 4 Materials and Methods

### 4.1 Cell and small animal x-ray irradiation system

The commissioning of x-ray irradiation systems for cells and small animals has been extensively studied [69]–[72]. The systems fall into two categories according to the type of source: a sealed gamma ray source or a sealed tube-based x-ray source [69], [73], [74]. X-ray irradiators use low-energy or medium-energy radiation and are usually self-contained and provide radiation protection for the user during irradiation. Good radiation protection and user friendliness make these systems good for research purposes [69], [75], [76].

The MultiRad 350 (Faxitron Bioptics, Tucson, AZ, USA) is a fully shielded, self-contained x-ray irradiation system. It uses a metal-ceramic x-ray tube capable of a maximum tube voltage of 350 kV (30-350 kV) and the tube current can be varied between 0.1 and 30 mA, but for a maximum tube voltage of 350 kV it is limited at 11.5 mA. The device has four different beam hardening filters: 0.5 mm and 2.0 mm Al, 0.3 mm Cu, and a combination of SnCuAl filters. The latter consists of 0.75 mm of Sn, 0.25 mm of Cu, and 1.50 mm of Al. The MultiRad 350 has a motorized shelf as a specimen holder and can be used to control the shelf-to-source distance between 13 cm and 65 cm. The shelf has an integrated internal IC that can be used for dose control and daily quality assurance procedures. In addition, the system is equipped with collimator jaws to limit the size of the x-ray beam. The maximum field size depends on the location of the shelf [77].

#### 4.1.1 Measurements with an x-ray irradiation system

Measurements with the x-ray irradiation system were divided into four parts: dose linearity and repeatability with irradiation time, CAX beam profiles, light field to irradiation field agreement, and absolute absorbed dose. All the measurements were performed at a distance of 45 cm from the shelf to the source.

Dose linearity and repeatability with irradiation time measurements were carried out with the internal IC of the x-ray system. Measurements were performed with a 0.5 mm Al filter and three different configurations: 350 kV and 10 mA, 250 kV and 14 mA, and 350 kV and 5 mA. Doses were recorded for irradiation times of 2 to 60 s.

The maximum tube potential of 350 kV with 10 mA tube current was chosen in such a way that the results would be close to the maximum doses and that the x-ray tube would not be overloaded.

CAX dose profiles were measured using radiochromic films (Gafchromic EBT3, Ashland). Axial profiles were collected using a field size of  $20 \times 20 \text{ cm}^2$  at the top of a 5.2 cm thick PMMA phantom to include backscatter.

For measurements of the agreement of the light field and irradiation field, field sizes of  $5 \times 5 \text{ cm}^2$ ,  $10 \times 10 \text{ cm}^2$ , and  $15 \times 15 \text{ cm}^2$  were recorded with radiochromic films. The corners of the corresponding light fields were marked on each film.

Absolute absorbed dose measurements were performed with RPLDs, radiochromic films, and a thimble IC (PTW30013, PTW-Freiburg GmbH, Freiburg, Germany). Both types of RPLD, GD-302M, and GD-352M were used. Measurements were carried out using a small water phantom ( $28.0 \times 28.0 \times 9.5 \text{ cm}^3$ ) at 0, 2, and 5 cm depths in water and 350 kV tube voltage, 10 mA tube current, and  $10 \times 10 \text{ cm}^2$  field size. Since the dose at 0 cm depth cannot be reliably measured by IC, the dose was extrapolated from the dose at 2 cm depth using the percentage depth dose (PDD) curve from the MultiRad manual and the results based on RPLD and film measurements.

## 4.2 Total body x-ray irradiation

TBI plays an essential role in the treatment of patients with acute myeloid or lymphoid leukemia undergoing hematopoietic stem cell transplantation [78]. The purpose is to immunosuppress the patient's entire bone marrow with ionizing radiation. This is to avoid donor bone marrow transplant rejection [79]. TBI is an alternative to medication methods such as chemotherapy. Usually, patients undergo either method or a combination of the two [78], [80], [81].

In this study, the TrueBeam (Varian Medical Systems Inc., now merged with Siemens Healthineers) linac was used as the treatment unit. The study investigates the anterior-posterior/posterior-anterior treatment technique, where the patient either lies on the couch on their back or side or remains standing with the SSD extended to 400 cm.

### 4.2.1 Measurements for total body x-ray irradiation

Dose measurements in this study were divided into three sections: PDD curves and CAX dose profiles in water, absolute absorbed dose in water, and point dose measurements in an anthropomorphic phantom. All measurements were performed using an SSD of 400 cm and a photon beam with a nominal energy of 6 MV. All field size data are projected field sizes for an SSD of 400 cm.

Measurements of PDD curves and CAX dose profiles were carried out using a water phantom (BP2, IBA Blue Phantom 2, IBA Dosimetry GmbH, Schwarzenbruck, Germany). Two identical ICs (IBA CC13, IBA Dosimetry GmbH) were used simultaneously, one to measure and one to correct for changes in readout caused by fluctuations in the linac output. Additionally, PDDs were measured with RPLDs (GD-302M) between depths of 1.5 cm and 30.0 cm. PDD measurements used a field size of  $160.0 \times 160.0 \text{ cm}^2$  and a collimator angle (CA) of  $45^\circ$ . For more accurate surface dose and maximum dose results, PDD curves were also measured in solid water slabs (Solid Water HE, Gammex, rebranded as Sun Nuclear, Middleton, WI, USA) with a density of  $1.032 \text{ g/cm}^3$ . Solid water measurements were performed using a parallel plate IC (IBA PPC40) at depths of 0.2–10.0 cm.

CAX dose profiles were measured with field sizes of  $10.0 \times 10.0 \text{ cm}^2$ ,  $20.0 \times 20.0 \text{ cm}^2$ , and  $30.0 \times 30.0 \text{ cm}^2$  at depths of 2.0, 10.0, and 20.0 cm using a CA of  $0^\circ$ . Additionally, the central region of both diagonal profiles was obtained at a depth of 10.0 cm using a field size of  $160.0 \times 160.0 \text{ cm}^2$  and a CA of  $45^\circ$ .

For absolute absorbed dose measurements, a thimble IC (PTW30013, PTW-Freiburg GmbH) was used in three different phantoms: BP2, a small water phantom ( $30 \times 30 \times 30 \text{ cm}^3$ ), and a self-made lung phantom. In BP2, the dose was obtained at two depths, 10.0 cm and 20.0 cm, and in the small water phantom from 10.0 cm depth. In the lung phantom, the dose was measured at a depth of 12.0 cm. A nominal dose of 300 monitor units (MU) was measured using a field size of  $10.0 \times 10.0 \text{ cm}^2$  and a nominal dose rate of 400 MU/min. Small water phantom measurements were repeated with RPLDs to determine correction factors for the RPLD energy response. The results were used with the IC results to calculate the correction factor.

TBI treatment was simulated using an anthropomorphic phantom (CIRS ATOM Model 701-C Adult Male Dosimetric Phantom, Computerized Imaging Reference Systems, Inc., Norfolk, VA, USA). A CT image dataset of the phantom was acquired in the head-first left decubitus position and treatment was planned using Eclipse (Varian Medical Systems Inc., now merged with Siemens Healthineers) TPS, a treatment dose of 2 Gy per fraction in the whole body volume with a field size of  $160.0 \times 160.0 \text{ cm}^2$ , and a CA of  $45^\circ$ . Inside the phantom, 45 RPLDs were placed throughout the phantom volume.

## 4.2.2 Simulations for total body x-ray irradiation

Two dose calculation algorithms were used in this study: AAA calculations (v15.6.04, Varian Medical Systems Inc., now merged with Siemens Healthineers) and MC simulations. The AAA calculations were performed with Eclipse TPS and the MC simulations with EGSnrc-based BEAMnrc and DOSXYZnrc simulations. The phantoms used in both calculations were created as precisely as possible in the

respective software. In the BEAMnrc simulation, the TrueBeam linac and the 6 MV photon beam were modeled according to the manufacturer's proprietary information. The source of the simulation was 6 MV phsp files published by the manufacturer. The Phsp file data were scored above the jaws. Due to the location of the phsp plane, the TrueBeam model contains only necessary parts below this plane. The model includes jaws, an approximation of the collimator baseplate, an MLC in the park position, and a light field reticle.

CT images were used in calculation of doses in the anthropomorphic phantom. The treatment plan was first calculated with AAA and then the same plan was imported with CT images into the MC software and re-calculated. After simulation, the MC plan was imported into Eclipse to collect the absorbed doses. Corresponding structures for the RPLDs were contoured in Eclipse for dose comparison.

## 4.3 Keloid scar gamma ray irradiation

Keloid is a pathological process in which the growth of wound healing scars is abnormal. It is usually elevated, pruritic, and painful and it can be a psychological burden for the patient [82]. This study investigated a treatment method in which a treatment catheter is surgically inserted into the scar after keloid removal and no bolus material is placed in the treatment area during RT.

The purpose of this study was to measure doses from two HDR afterloader units: microSelectron V2 (Elekta AB, Stockholm, Sweden) and Bravos (Varian Medical Systems Inc., now merged with Siemens Healthineers). Both treatment units use the Ir-192 source: microSelectron-v2 and GammaMed Plus (Model 232), respectively.

### 4.3.1 Measurements for keloid scar gamma ray irradiation

The plan used in the keloid scar dose measurements consisted of 30 dwell positions with 0.5 cm step size, simulating a 15 cm long surgically removed scar (surgical cavity) treatment. This plan was created with Eclipse BrachyVision (v16.1, Varian Medical Systems Inc.) TPS using the AAPM Task Group No. 43 (TG-43) dose model [83]. The dose was normalized to 8.5 Gy at a distance of 0.5 cm from the center of the sources.

In this study, GD-302M type RPLDs were used. Measurements were carried out on solid water slabs (Gammex®,  $35.3 \times 36.7 \text{ cm}^2$ ) with variable thickness and polycarbonate (PC) sheet (Makrolon®,  $26.0 \times 26.0 \text{ cm}^2$ ) with a thickness of 0.6 cm. There were five different measurement setups for measuring the dose at three depths. The setups were as follows:

- 1) Top PC sheet with positions for the RPLDs and treatment catheter. Four RPLDs placed at a distance of 0.5 cm and four at 1.0 cm from the center of the

catheter. In the second PC sheet, five RPLDs under the catheter at a distance of 0.65 cm. Figure 11a shows the measurement setup.

2) Top PC sheet with a position for the catheter. Next a 0.5 cm thick solid water slab and below that a PC sheet with five RPLDs at a distance of 1.15 cm.

3) The same PC sheet with the catheter and a blank sheet underneath. Between the sheets, one sheet of EBT3 film (Figure 11b).

4) Top: PC sheet with catheter, next 0.5 cm of solid water and EBT3 film underneath.

5) The same setup as in 4), but the thickness of the solid water changed to 1.0 cm. Each measurement setup was placed between 0.2 cm thick and approximately 18 cm thick solid water slabs to simulate skin and internal body structures (Figure 12a). Measurements were made in exactly the same way in both treatment units.

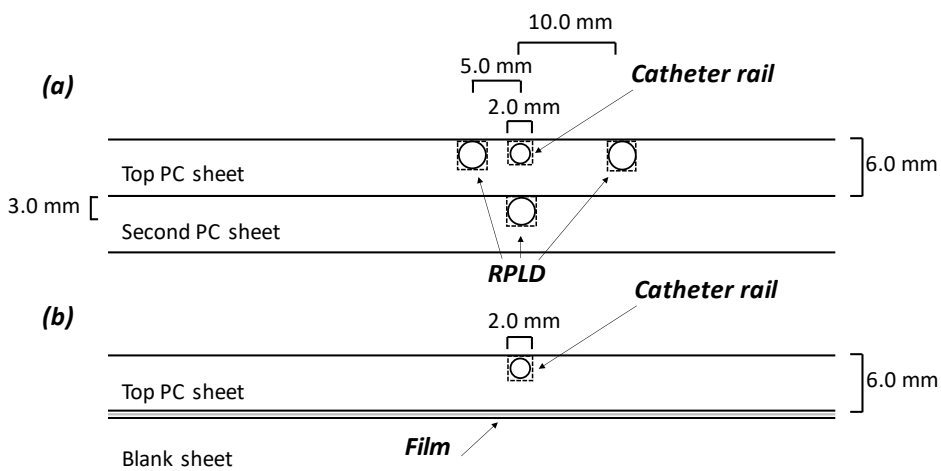


**Figure 11.** Schematic representation of the cross-sections of polycarbonate (PC) sheets in (a) RPLD and (b) film measurements. PC sheets were placed between 0.2 cm thick and approximately 18 cm thick solid water slabs (RPLD: radiophotoluminescence dosimeter) [III].

### 4.3.2 Simulations for keloid scar gamma ray irradiation

In this study, simulations were performed using `egs_brachy`. The corresponding PC sheets and solid water slabs were modeled as accurately as possible according to the material data. Three different simulations were performed in both treatment units.

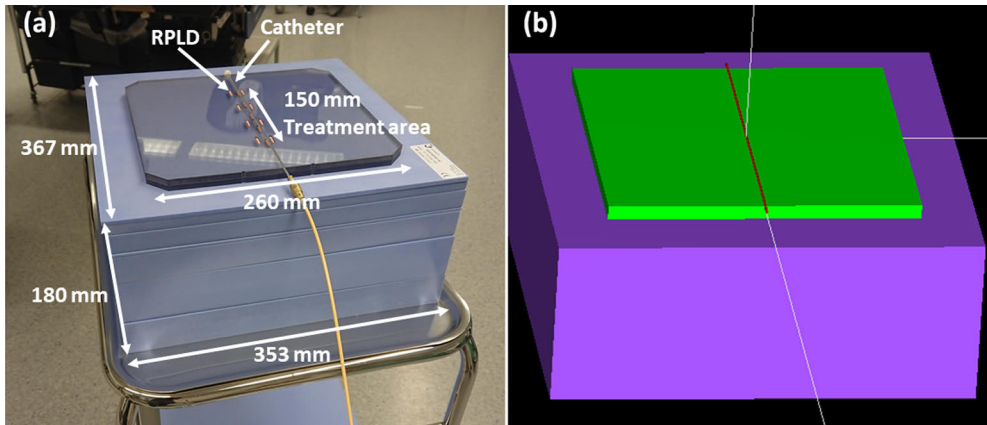


**Figure 12.** (a) Measurement phantom made of polycarbonate (PC) and solid water. (b) Phantom modeled with `egs_brachy`. The figures are missing 0.2 cm solid water slabs for better illustration (RPLD: radiophotoluminescence dosimeter) [III].

1) Modeled 1.2 cm thick PC matrix for scoring. This was for comparison with RPLD measurements at distances of 0.5, 0.65, and 1.0 cm and film measurements at a depth of 0.5 cm (Figure 12b).

2) Two 0.6 cm thick PC sheets were modeled, the first being a block and the second a matrix, with 0.5 cm thick solid water between the PC sheets. This was compared with the RPLD measurement at a distance of 1.15 cm.

3) One 0.6 cm thick PC sheet on top and a 1.5 cm thick solid water matrix below it were modeled for comparison with the film measurement at depths of 1.0 and 1.5 cm.

In each simulation, the grid size of the scoring matrix was  $0.1 \times 0.1 \times 0.05 \text{ cm}^3$ , configurations were placed between 0.2 cm thick and approximately 18 cm thick solid water slabs, and the created phantoms were placed in the middle of a  $400 \times 400 \times 400 \text{ cm}^3$  air cube. In the upper PC sheet, the catheter was modeled as a hollow 0.2 cm thick and 16.0 cm long cylinder made of PMMA. The phantom models were placed so that the center of the x-axis was in the middle of the cylinder and the source moved along the axis. Sources from the `egs_brachy` library, `microselectron-v2`, and `MBDCA-WG` were used with `microSelectron` and `Bravos`, respectively. The simulations were run separately with both sources. The correction factor was calculated according to the `egs_brachy` manual and implemented to scale the dose to be comparable with the measurements. More information about the simulation parameters can be found in Study III.

In order to compare the treatment plans, film measurements, and MC simulations, profiles were created with Eclipse TPS, where the plans were calculated with the TG-43 algorithm in water. The plans were also re-calculated using Eclipse's

Acuros BV (v. 1.8.0.867816) dose calculation algorithm, which is a more modern algorithm used in clinical TPS.

## 5 Summary of the Results (I-III)

The original publications included in this thesis deal with methods of measuring and calculating the absorbed dose delivered by x-ray and gamma radiation. The main aspects of the work lay in the development of experimental methods. The experimental setups employed in Studies **I** and **II** took advantage of x-rays produced in two different ways, characteristic radiation from an x-ray tube (30–350 kV) and bremsstrahlung radiation from a linac (6 MV), while the experimental setup employed in Study **III** exploited the use of gamma radiation from a sealed Ir-192 source (206–612 keV).

**I.** The results show that the dose was linear at each voltage setting applied, and the results were reproducible within 5 % after 15 s of irradiation time. The x-ray beam profiles were at an acceptable level in line with the manufacturer's specifications, and the light field had shifted by about 0.5 cm.

**II.** The calculated and measured PDD curves and CAX profiles were found to be clinically acceptable, and a small overestimation of the calculated results (MC: 2.2 %, and AAA: 1.8 %) compared with the absolute absorbed dose measurements was observed. The point dose results measured with RPLDs in the anthropomorphic phantom showed good agreement between the measurements and MC simulations, with an average difference of only 1.0 % (0–2.1 %) in the whole-body volume. In contrast, the AAA calculation appeared to overestimate the doses, the results for the whole-body volume being 6.2 % higher than in the measurements. In smaller body volumes the difference was even larger (head 8.3 %).

**III.** The dose profiles agreed well between measurements and calculations; only a small difference of less than 4 % was observed. Point dose measurements agreed well in the dose maximum area (difference < 7 %) with the simulated dose profiles, although the largest difference near the edge of the profile was < 30 %. The dose differences between the TG-43 dose model and the MC simulation were small (< 4 %).

## 6 Discussion

The aim of Study I was to describe the commissioning process of an x-ray irradiator, i.e., to determine the beam characteristics and dose delivery. Similar irradiation systems have been investigated by Newton *et al.* [69], Stojadinovic *et al.* [70], and Wang *et al.* [84]. The system uses low- or medium-energy kilovoltage x-rays with several filter options, allowing the study of the use of these energies.

Energy dependence of both RPLD types was observed in the measurements. The doses measured with GD-302M (RPLDs without Sn filter) were twice as high as with IC doses when the thinnest Al filter was used. With GD-352M, this effect was not observed, as the dose difference was only about 15 %, which was in the expected range. When using the thickest filter, the difference was 12 % for GD-302M and 23 % for GD-352M in comparison to IC. The same trend can also be seen in comparison to the film results. These results are in good agreement with the energy dependence curve (Figure 4). The results show that the energy of the radiation beam must be taken into account when planning dose measurements. It also shows that when aiming for the most accurate results, the calibration factor of RPLDs should be calculated individually for each measurement, rather than using a factory calibration or a generic value, especially if the applied energy changes.

The results of this study with the MultiRad 350 x-ray irradiation system show that the system works as expected except for two things: the minimum acceptable irradiation time is 15 s, which must be taken into account when the planned dose is less than 1 Gy, and an exceptionally small target should not be irradiated or use small fields before calibrating the light field and the irradiation field.

The main aim of Study II was to evaluate the suitability of AAA implemented in the Varian Eclipse TPS for TBI treatments when using an extended SSD of 400 cm. Similar studies have been conducted by Lamichhane *et al.* [85] & [86], Hussain *et al.* [87], and Tyson *et al.* [88], with relatively similar results to ours, but one study did not recommend AAA for TBI calculation. There, additionally to these four studies, the results of the AAA calculation were also compared with results of the MC simulations.

In this study, the models, MC simulations, and their accuracy were important. In the first two parts of study, the simulation model consisted of a linac and a water

phantom, while in the last part it consisted of a linac and a body phantom. There are only slight discrepancies in these simulated parts compared with the real-life measurements, but they are hard to correct (mechanical inaccuracy of the jaws) or would take too much time to do so (the inclusion of furniture and walls to the simulation), and the benefits would be small. The difference in dose definition between the AAA and MC simulations (dose-to-water compared with dose-to-medium) increased the differences in the absolute absorbed dose results. This difference is acceptable if the MC model is to match reality as well as possible. The dose definition cannot be changed in the AAA calculation. As seen in the last part of the study, these same effects do not occur in the treatment scenario when the simulation model consists of the linac and body phantom. The small size and correction factors of the RPLD enabled accurate point measurements in the anthropomorphic body phantom. The RPLDs could be arranged freely in the phantom grid, allowing the measurements of absorbed dose in organ-specific regions. The size of the RPLD also creates a small challenge, because the results are point-like and do not tell the whole truth about the dose distribution.

The aim of Study III was to determine the feasibility and accuracy of the absorbed dose by the HDR afterloader in keloid scar BT. In addition, the study aimed to investigate the accuracy of the TG-43 algorithm used in clinical treatment planning. This was performed using MC simulations and measurements. Finally, the measurements and MC simulations were compared with the Acuros BV algorithm, which represents the latest generation of BT dose calculation algorithms.

In this study, similar problems were observed in the MC simulations to those in Study II. Small differences were observed due to dose definition, in the dose-to-water calculation versus dose-to-medium calculation. The differences in the properties of the modeled medium (PC) and the material used were also unknown. Large differences were observed for RPLD results compared with MC results. The observed differences were probably due to the poor placement accuracy of the measurement configuration and the RPLDs. The largest differences were observed near the penumbra region, where the placement is most sensitive. In addition, measurements with an HDR source are very sensitive to the distances between dosimeters and the source, the sensitivity becoming more critical closer to the source. In the measurements, the processing was manually aligned, which only affects the accuracy of the RPLD results, as all the profiles were independently centered using the calculated full width at half maximum of the profile. Some of the differences between simulations and measurements can be explained by gravity (the source moves by touching the inner surface of the catheter), which the simulations do not consider.

These studies show that the design of measurements and correction factors is important when using RPLDs. Although RPLDs are quite easy to use, the location

of the dosimeters should be carefully validated. MC simulations give accurate results, but still the model used should be carefully constructed so that it matches reality as accurately as possible. Despite this, problems may arise with the materials or dose definition. But when both methods are successfully combined into a measurement setup, the results enable accurate development work.

# 7 Conclusions

In this thesis, RPLDs were investigated in the verification of absorbed dose with different irradiation energies in various geometries, and the results measured by RPLDs were compared with the results calculated by the MC method. The research was divided into three parts, each focusing on different geometries, radiation treatment modalities, and beam qualities. The results suggest that RPLDs are versatile and fairly easy-to-use dosimeters that are suitable for many different purposes. The accuracy of MC simulations is widely known, although the results can only be as accurate as the model used. Both methods have their strengths and weaknesses, but together they complement each other. Based on the results presented in the original publications (I-III), the following conclusions can be drawn:

**I:** The x-ray irradiation system can be used safely and in a controlled manner to irradiate cells and small animals. However, positioning of the filter must be carefully checked between each change.

**II:** The AAA calculation can be safely used in TBI treatment planning with an extended SSD of 400 cm. However, to achieve greater accuracy to within 5 % in the planning of TBI treatment, dose validation of TPS must be performed carefully at extended SSDs.

**III:** The nominal treatment dose can be achieved to an accuracy of 4 % with the utilized setup. The calculation accuracy of TG-43 seems to decrease with increasing distance from the source, which does not significantly affect the treatment of keloid scars. It was observed that the placement of RPLDs requires special attention.

For the most accurate results, RPLDs must be corrected against a known dosimeter, such as an IC. These correction factor measurements should be performed individually per measurement in a known setup and conditions, e.g., a water phantom that is as similar as possible to the actual dose measurements. Correction can be made directly to the RPLD reader or with a correction factor. Using a correction

factor also corrects the energy dependencies of the RPLD. This also leaves more options for the user to measure doses in different setups, because the correction by the manufacturer is intact. The use of RPLDs should be planned in advance: which RPLD model to use, with what layout and attachment to the phantom.

MC simulation gives the user freedom to simulate or calculate doses in different setups with the highest accuracy. It brings new perspectives to solving problems, even when they are not directly detectable with the dose measurements. The MC dose calculation results provide a theoretical comparison to the dose measurements, which adds more value to the research. When creating a phantom, even with special care a perfect model cannot be achieved due to the random nature of materials. This process can be accelerated using CT-based MC simulations, which has its own challenges. Overall, MC simulations are a versatile method that can be used in a variety of research setups.

# List of References

- [1] A. Kosunen, P. Sipilä, R. Parkkinen, I. Jokelainen, and H. Järvinen, “Ulkoisen sädehoidon suurenergisten foton- ja elektronisäteilykeilojen kalibrointi,” in *Sädehoidon annosmittaukset*, Vantaa: Säteilyturvakeskus, 2005.
- [2] S. F. Kry *et al.*, “AAPM TG 191: Clinical use of luminescent dosimeters: TLDs and OSLDs,” *Med. Phys.*, vol. 47, no. 2, pp. e19–e51, Feb. 2020, doi: 10.1002/MP.13839.
- [3] D. Y. C. Huang and S.-M. Hsu, “Radio-Photoluminescence Glass Dosimeter (RPLGD),” in *Advances in Cancer Therapy*, InTech, 2011.
- [4] J. Bancheri, S. Ketelhut, L. Büermann, and J. Seuntjens, “Monte Carlo and water calorimetric determination of kilovoltage beam radiotherapy ionization chamber correction factors,” *Phys. Med. Biol.*, vol. 65, no. 10, p. 105001, May 2020, doi: 10.1088/1361-6560/ab82e7.
- [5] X. Chen *et al.*, “A novel design of proton computed tomography detected by multiple-layer ionization chamber with strip chambers: A feasibility study with Monte Carlo simulation,” *Med. Phys.*, vol. 47, no. 2, pp. 614–625, Feb. 2020, doi: 10.1002/mp.13909.
- [6] T. Han, J. K. Mikell, M. Salehpour, and F. Mourtada, “Dosimetric comparison of Acuros XB deterministic radiation transport method with Monte Carlo and model-based convolution methods in heterogeneous media,” *Med. Phys.*, vol. 38, no. 5, pp. 2651–2664, May 2011, doi: 10.1118/1.3582690.
- [7] H. D. Young, R. A. Freedman, and A. L. Ford, *Sears and Zemansky’s University Physics : with modern physics.*, 13th ed. San Francisco: Pearson, 2008.
- [8] O. Marttila, “Suureet ja yksiköt,” in *Säteily ja sen havaitseminen*, T. K. Ikäheimonen, Ed. Hämeenlinna: Säteilyturvakeskus, 2002, pp. 66–91.
- [9] P. Sipilä, “Sädehoito,” in *Säteilyn käyttö*, O. Pukkila, Ed. Hämeenlinna: Säteilyturvakeskus, 2004, pp. 184–217.
- [10] J. Seuntjens, M. Olivares, M. Evans, and E. Podgorsak, “Absorbed dose to water reference dosimetry using solid phantoms in the context of absorbed-dose protocols,” *Med. Phys.*, vol. 32, no. 9, pp. 2945–2953, Sep. 2005, doi: 10.1118/1.2012807.
- [11] S. Pojtinger, O. S. Dohm, R. P. Kapsch, and D. Thorwarth, “Ionization chamber correction factors for MR-linacs,” *Phys. Med. Biol.*, vol. 63, no. 11, p. 11NT03, Jun. 2018, doi: 10.1088/1361-6560/aac4f2.
- [12] C. J. Hourdakos *et al.*, “Comparison of pencil-type ionization chamber calibration results and methods between dosimetry laboratories,” *Phys. Medica*, vol. 32, no. 1, pp. 42–51, Jan. 2016, doi: 10.1016/j.ejmp.2015.09.008.
- [13] J. Navarro Campos, J. de Pooter, L. de Prez, and B. Jansen, “The impact of ion chamber components on k B,Q for reference dosimetry in MRgRT,” *Phys. Med. Biol.*, vol. 67, no. 14, p. 145001, Jul. 2022, doi: 10.1088/1361-6560/ac77d0.
- [14] S. Klemola, “Säteilyn ilmaisimet,” in *Säteily ja sen havaitseminen*, T. K. Ikäheimonen, Ed. Hämeenlinna: Säteilyturvakeskus, 2002, pp. 116–134.
- [15] M. R. McEwen and J. Taank, “Examining the influence of humidity on reference ionization chamber performance,” *Med. Phys.*, vol. 44, no. 2, pp. 694–702, Feb. 2017, doi: 10.1002/mp.12057.

- [16] C. K. Spindeldreier *et al.*, “Radiation dosimetry in magnetic fields with Farmer-type ionization chambers: Determination of magnetic field correction factors for different magnetic field strengths and field orientations,” *Phys. Med. Biol.*, vol. 62, no. 16, pp. 6708–6728, Aug. 2017, doi: 10.1088/1361-6560/aa7ae4.
- [17] International Atomic Energy Agency IAEA, “Absorbed Dose Determination in External Beam Radiotherapy: An International Code of Practice for Dosimetry Based on Standards of Absorbed Dose to Water,” in *Technical Reports Series No. 398*, Vienna, 2000.
- [18] M. Tapiovaara, O. Pukkila, and A. Miettinen, “Röntgensäteily diagnostiikassa,” in *Säteilyn käyttö*, O. Pukkila, Ed. Hämeenlinna: Säteilyturvakeskus, 2004, pp. 1–180.
- [19] C.-M. Ma *et al.*, “AAPM protocol for 40-300 kV x-ray beam dosimetry in radiotherapy and radiobiology,” *Med. Phys.*, vol. 28, no. 6, pp. 868–893, Jun. 2001, doi: 10.1118/1.1374247.
- [20] M. A. Omary and H. H. Patterson, “Luminescence, Theory,” in *Encyclopedia of Spectroscopy and Spectrometry*, 3rd ed., J. Lindon, G. E. Tranter, and D. Koppenaal, Eds. Elsevier, 2017, pp. 636–653.
- [21] N. S. Bajaj, C. B. Palan, V. Chopra, and S. J. Dhoble, “An introduction to radio-photoluminescence and scintillation for dosimetric applications,” in *Radiation Dosimetry Phosphors*, 1st ed., S. J. Dhoble, V. Chopra, V. Nayar, G. Kitis, D. Poelman, and H. Swart, Eds. Elsevier Inc., 2022, pp. 431–454.
- [22] S.-M. Hsu, S.-H. Yeh, M.-S. Lin, and W.-L. Chen, “Comparison on characteristics of radiophotoluminescent glass dosimeters and thermoluminescent dosimeters,” *Radiat. Prot. Dosimetry*, vol. 119, no. 1–4, pp. 327–331, Sep. 2006, doi: 10.1093/rpd/nci510.
- [23] F. Araki, N. Moribe, T. Shimonobou, and Y. Yamashita, “Dosimetric properties of radiophotoluminescent glass rod detector in high-energy photon beams from a linear accelerator and Cyber-Knife,” *Med. Phys.*, 2004, doi: 10.1118/1.1758351.
- [24] S. M. Hsu *et al.*, “Clinical application of radiophotoluminescent glass dosimeter for dose verification of prostate HDR procedure,” *Med. Phys.*, vol. 35, no. 12, pp. 5558–5564, Nov. 2008, doi: 10.1118/1.3005478.
- [25] J. H. Lee, M. S. Lin, S. M. Hsu, I. J. Chen, W. L. Chen, and C. F. Wang, “Dosimetry characteristics and performance comparisons: Environmental radiophotoluminescent glass dosimeters versus thermoluminescent dosimeters,” *Radiat. Meas.*, vol. 44, no. 1, pp. 86–91, Jan. 2009, doi: 10.1016/j.radmeas.2008.10.013.
- [26] F. Araki and T. Ohno, “The response of a radiophotoluminescent glass dosimeter in megavoltage photon and electron beams,” *Med. Phys.*, vol. 41, no. 12, p. 122102, Dec. 2014, doi: 10.1118/1.4901639.
- [27] “GD-300 series Instruction Manual,” Shizuoka, Japan, Feb. 2012.
- [28] K. Fujii *et al.*, “Correlation analysis of organ doses determined by Monte Carlo simulation with dose metrics for patients undergoing chest-abdomen-pelvis CT examinations,” *Phys. Medica*, vol. 77, pp. 1–9, Sep. 2020, doi: 10.1016/j.ejmp.2020.07.016.
- [29] C. Nakatake and F. Araki, “Energy response of radiophotoluminescent glass dosimeter for diagnostic kilovoltage x-ray beams,” *Phys. Medica*, vol. 82, pp. 144–149, Feb. 2021, doi: 10.1016/j.ejmp.2021.01.076.
- [30] H. Vincke *et al.*, “Response of alanine and radio-photo-luminescence dosimeters to mixed high-energy radiation fields,” *Radiat. Prot. Dosimetry*, vol. 125, no. 1–4, pp. 340–344, Dec. 2006, doi: 10.1093/rpd/ncm157.
- [31] A. L. Manninen, A. Koivula, and M. T. Nieminen, “The applicability of radiophotoluminescence dosimeter (RPLD) for measuring medical radiation (MR) doses,” *Radiat. Prot. Dosimetry*, vol. 151, no. 1, pp. 1–9, Aug. 2012, doi: 10.1093/rpd/ncr463.
- [32] J. Nandha Gopal, B. Sanyal, and A. Lakshmanan, “Radiophotoluminescence and thermoluminescence characteristics of undoped and Mg doped LiF phosphor in the high dose region,” *Radiat. Meas.*, vol. 109, pp. 24–34, Feb. 2018, doi: 10.1016/j.radmeas.2017.12.007.
- [33] “FGD-1000 Instruction Manual, Ver.2,” Shizuoka, Japan, Dec. 2011.

- [34] W. Chang *et al.*, “Correction of stopping power and LET quenching for radiophotoluminescent glass dosimetry in a therapeutic proton beam,” *Phys. Med. Biol.*, vol. 62, no. 23, p. 8869, Nov. 2017, doi: 10.1088/1361-6560/AA9155.
- [35] S.-M. Hsu *et al.*, “Synthesis and physical characteristics of radiophotoluminescent glass dosimeters,” *Radiat. Meas.*, vol. 42, no. 4–5, pp. 621–624, Apr. 2007, doi: 10.1016/j.radmeas.2007.01.053.
- [36] J. Seco and F. Verhaegen, *Monte Carlo Techniques in Radiation Therapy*. Boca Raton: Taylor & Francis Group, 2013.
- [37] I. J. Chetty *et al.*, “Report of the AAPM Task Group No. 105: Issues associated with clinical implementation of Monte Carlo-based photon and electron external beam treatment planning,” *Med. Phys.*, vol. 34, no. 12, pp. 4818–4853, Nov. 2007, doi: 10.1118/1.2795842.
- [38] I. Kawrakow, E. Mainegra-Hing, D. W. O. Rogers, F. Tessier, and B. R. B. Walters, “EGSnrc: software for Monte Carlo simulation of ionizing radiation,” *Natl. Res. Counc. Canada*, 2000, doi: 10.4224/40001303.
- [39] I. Kawrakow, E. Mainegra-Hing, D. W. O. Rogers, F. Tessier, and B. R. B. Walters, “The EGSnrc Code System: Monte Carlo Simulation of Electron and Photon Transport, NRCC Report PIRS-701,” *Natl. Res. Counc. Canada*, pp. 2001–2019, 2019.
- [40] M. Partanen, J. Niemelä, J. Ojala, J. Keyriläinen, and M. Kapanen, “Properties of IBA Razor Nano Chamber in small-field radiation therapy using 6 MV FF, 6 MV FFF, and 10 MV FFF photon beams,” *Acta Oncol. (Madr)*, vol. 60, no. 11, pp. 1419–1424, Nov. 2021, doi: 10.1080/0284186X.2021.1979644.
- [41] “Definition of phase-space (phsp) data,” *International Atomic Energy Agency - Nuclear Data Section*, 2013. [https://www-nds.iaea.org/phsp/documents/phsp\\_definition.htm](https://www-nds.iaea.org/phsp/documents/phsp_definition.htm) (accessed Aug. 16, 2022).
- [42] M. Ghazal, L. Södergren, M. Westermark, J. Söderström, and T. Pommer, “Dosimetric and mechanical equivalency of Varian TrueBeam linear accelerators,” *J. Appl. Clin. Med. Phys.*, vol. 21, no. 12, pp. 43–53, Dec. 2020, doi: 10.1002/acm2.13058.
- [43] G. Narayanasamy, D. Saenz, W. Cruz, C. S. Ha, N. Papanikolaou, and S. Stathakis, “Commissioning an Elekta Versa HD linear accelerator,” *J. Appl. Clin. Med. Phys.*, vol. 17, no. 1, pp. 179–191, Jan. 2016, doi: 10.1120/jacmp.v17i1.5799.
- [44] D. W. O. Rogers, B. A. Faddegon, G. X. Ding, C.-M. Ma, J. We, and T. R. Mackie, “BEAM: A Monte Carlo code to simulate radiotherapy treatment units,” *Med. Phys.*, vol. 22, no. 5, pp. 503–524, May 1995, doi: 10.1118/1.597552.
- [45] B. Walters, I. Kawrakow, and D. W. O. Rogers, “DOSXYZnrc Users Manual, NRCC Report PIRS-0794,” *Natl. Res. Counc. Canada*, pp. 1–132, 2021.
- [46] J. R. Treurniet, B. R. Walters, I. Kawrakow, and D. W. O. Rogers, “BEAMnrc, DOSXYZnrc and BEAMDP GUI User’s Manual, NRCC Report PIRS-0623(rev C),” Ottawa, 2018.
- [47] D. W. O. Rogers, B. Walters, and I. Kawrakow, “BEAMnrc Users Manual, NRCC Report PIRS-0509(A)revL,” *Natl. Res. Counc. Canada*, pp. 1–301, 2021.
- [48] N. Wen *et al.*, “IMRT and RapidArc commissioning of a TrueBeam linear accelerator using TG-119 protocol cases,” *J. Appl. Clin. Med. Phys.*, vol. 15, no. 5, pp. 74–88, Sep. 2014, doi: 10.1120/jacmp.v15i5.4843.
- [49] C. Glide-Hurst *et al.*, “Commissioning of the Varian TrueBeam linear accelerator: A multi-institutional study,” *Med. Phys.*, vol. 40, no. 3, p. 031719, Mar. 2013, doi: 10.1118/1.4790563.
- [50] S. Palled, S. Saminathan, T. Pasha, T. Naveen, K. Ganesh, and V. Lokesh, “Prostate permanent implant brachytherapy with BARC I-125 Ocu-Prosta seeds,” *J. Cancer Res. Ther.*, vol. 17, no. 2, pp. 340–347, Apr. 2021, doi: 10.4103/jcrt.JCRT\_424\_20.
- [51] C. H. Holschneider *et al.*, “Brachytherapy: A critical component of primary radiation therapy for cervical cancer,” *Gynecol. Oncol.*, vol. 152, no. 3, pp. 540–547, Mar. 2019, doi: 10.1016/j.ygyno.2018.10.016.

- [52] A. A. Weiner and J. K. Schwarz, "Intracavitary Brachytherapy for Gynecologic Malignancies: Applications and Innovations," *Mo. Med.*, vol. 112, no. 5, p. 366, Sep. 2015, Accessed: Jan. 26, 2023. [Online]. Available: </pmc/articles/PMC6167241/>.
- [53] S. Lettmaier and V. Strnad, "Intraluminal brachytherapy in oesophageal cancer: defining its role and introducing the technique," *J. Contemp. Brachytherapy*, vol. 6, no. 2, p. 236, 2014, doi: 10.5114/JCB.2014.43780.
- [54] S. Cozzi *et al.*, "The Role of Interstitial Brachytherapy for Breast Cancer Treatment: An Overview of Indications, Applications, and Technical Notes," *Cancers (Basel)*, vol. 14, no. 10, May 2022, doi: 10.3390/CANCERS14102564.
- [55] M. Bellezzo, J. A. Baeza, R. Voncken, B. Reniers, F. Verhaegen, and G. P. Fonseca, "Mechanical evaluation of the Bravos afterloader system for HDR brachytherapy," *Brachytherapy*, vol. 18, no. 6, pp. 852–862, Nov. 2019, doi: 10.1016/J.BRACHY.2019.06.005.
- [56] D. Tho, M. Lavallée, and L. Beaulieu, "Performance of an enhanced afterloader with electromagnetic tracking capabilities for channel reconstruction and error detection," *Med. Phys.*, vol. 48, no. 8, pp. 4402–4410, Aug. 2021, doi: 10.1002/mp.14877.
- [57] M. J. P. Chamberland, R. E. P. Taylor, D. W. O. Rogers, and R. M. Thomson, "Egs-brachy: A versatile and fast Monte Carlo code for brachytherapy," *Phys. Med. Biol.*, vol. 61, no. 23, pp. 8214–8231, 2016, doi: 10.1088/0031-9155/61/23/8214.
- [58] I. Kawrakow, E. Mainegra-Hing, F. Tessier, R. Townson, and B. Walters, "EGSnrc C++ class library, NRC Report PIRS-898 (rev A)," *Natl. Res. Counc. Canada*, 2019.
- [59] T. Failing, G. H. Hartmann, F. W. Hensley, B. Keil, and K. Zink, "Enhancement of the EGSnrc code egs\_chamber for fast fluence calculations of charged particles," *Z. Med. Phys.*, May 2022, doi: 10.1016/j.zemedi.2022.04.003.
- [60] D. van Eeden and F. du Plessis, "EGS\_cbct: Simulation of a fan beam CT and RMI phantom for measured HU verification," *Phys. Medica*, vol. 32, no. 10, pp. 1375–1380, Oct. 2016, doi: 10.1016/j.ejmp.2016.09.011.
- [61] M. P. Martinov, C. Opara, R. M. Thomson, and T. Y. Lee, "Fast beta-emitter Monte Carlo simulations and full patient dose calculations of targeted radionuclide therapy: introducing egs\_mird," *Med. Phys.*, vol. 49, no. 9, pp. 6137–6149, Jun. 2022, doi: 10.1002/mp.15786.
- [62] R. M. Thomson, R. E. P. Taylor, M. J. P. Chamberland, and D. W. O. Rogers, "User manual for egs\_brachy: A versatile and fast EGSnrc application for brachytherapy," *Natl. Res. Counc. Canada*, pp. 1–42, 2017.
- [63] R. Taylor, M. Chamberland, D. Rogers, and R. Thomson, "EGS Brachy Technical Reference Manual," Ottawa, 2017.
- [64] Ashland Inc, "GAFCHROMIC™ DOSIMETRY MEDIA, TYPE EBT-3." Accessed: Jan. 24, 2023. [Online]. Available: [www.FilmQAPro.com](http://www.FilmQAPro.com).
- [65] E. Y. León Marroquin, J. A. Herrera González, M. A. Camacho López, J. E. Villarreal Barajas, and O. A. García-Garduño, "Evaluation of the uncertainty in an EBT3 film dosimetry system utilizing net optical density," *J. Appl. Clin. Med. Phys.*, vol. 17, no. 5, pp. 466–481, Sep. 2016, doi: 10.1120/JACMP.V17I5.6262.
- [66] A. Niroomand-Rad *et al.*, "Report of AAPM Task Group 235 Radiochromic Film Dosimetry: An Update to TG-55," *Med. Phys.*, vol. 47, no. 12, pp. 5986–6025, Dec. 2020, doi: 10.1002/MP.14497.
- [67] A. M. Flejmer, F. Dohlmair, M. Nilsson, M. Stenmarker, and A. Dasu, "Analytical anisotropic algorithm versus pencil beam convolution for treatment planning of breast cancer: implications for target coverage and radiation burden of normal tissue.," *Anticancer Res.*, vol. 35, no. 5, pp. 2841–8, May 2015, Accessed: Jan. 31, 2023. [Online]. Available: <https://pubmed.ncbi.nlm.nih.gov/25964565/>.
- [68] M. Sinnatamby, V. Nagarajan, R. K. Sathyanarayana, G. Karunanidhi, and V. Singhavajala, "Dosimetric comparison of Acuros™ BV with AAPM TG43 dose calculation formalism in breast interstitial high-dose-rate brachytherapy with the use of metal catheters," *J. Contemp. Brachytherapy*, vol. 7, no. 4, p. 273, 2015, doi: 10.5114/JCB.2015.54052.

- [69] J. Newton *et al.*, “Commissioning a small-field biological irradiator using point, 2D, and 3D dosimetry techniques,” *Med. Phys.*, vol. 38, no. 12, pp. 6754–6762, Dec. 2011, doi: 10.1118/1.3663675.
- [70] S. Stojadinovic *et al.*, “MicroRT—Small animal conformal irradiator,” *Med. Phys.*, vol. 34, no. 12, pp. 4706–4716, Dec. 2007, doi: 10.1118/1.2799887.
- [71] A. C. Bruno, S. J. Mazaro, L. L. Amaral, E. M. Rego, H. F. Oliveira, and J. F. Pavoni, “Biological X-ray irradiator characterization for use with small animals and cells,” *Brazilian J. Med. Biol. Res.*, 2017, doi: 10.1590/1414-431X20165848.
- [72] P. Kuess, E. Bozsaky, J. Hopfgartner, G. Seifritz, W. Dörr, and D. Georg, “Dosimetric challenges of small animal irradiation with a commercial X-ray unit,” *Z. Med. Phys.*, vol. 24, no. 4, pp. 363–372, Dec. 2014, doi: 10.1016/J.ZEMEDI.2014.08.005.
- [73] M. K. Ozbilgin, C. Aktas, E. T. Uluer, M. C. Buyukuysal, M. S. Gareveran, and C. Kurtman, “Influence of Radiation Exposure During Radiotherapy. Evidence for the Increase of Versican and Heparin-Binding EGF-like Growth Factor Concentrations,” *Anal. Quant. Cytopathol. Histopathol.*, vol. 38, no. 2, pp. 126–132, Apr. 2016.
- [74] G. Garty *et al.*, “VADER: a variable dose-rate external <sup>137</sup>Cs irradiator for internal emitter and low dose rate studies,” *Sci. Rep.*, vol. 10, no. 1, Dec. 2020, doi: 10.1038/s41598-020-76941-2.
- [75] R. Azimi, P. Alaei, E. Spezi, and S. K. Hui, “Characterization of an orthovoltage biological irradiator used for radiobiological research,” *J. Radiat. Res.*, vol. 56, no. 3, p. 485, 2015, doi: 10.1093/JRR/RRU129.
- [76] R. Clarkson *et al.*, “Characterization of image quality and image-guidance performance of a preclinical microirradiator,” *Med. Phys.*, vol. 38, no. 2, pp. 845–856, Jan. 2011, doi: 10.1118/1.3533947.
- [77] “MultiRad 350 User’s Manual,” May 2015.
- [78] J. Y. C. Wong, A. R. Filippi, B. S. Dabaja, J. Yahalom, and L. Specht, “Total Body Irradiation: Guidelines from the International Lymphoma Radiation Oncology Group (ILROG),” *International Journal of Radiation Oncology Biology Physics*, vol. 101, no. 3. Elsevier Inc., pp. 521–529, Jul. 2018, doi: 10.1016/j.ijrobp.2018.04.071.
- [79] F. M. Khan and J. P. Gibbons, *The Physics of Radiation Therapy*, 5th ed. Philadelphia: Lippincott Williams & Wilkins, 2014.
- [80] H. Rafei, H. M. Kantarjian, and E. J. Jabbour, “Recent advances in the treatment of acute lymphoblastic leukemia,” *Leuk. Lymphoma*, vol. 60, no. 11, pp. 2606–2621, Sep. 2019, doi: 10.1080/10428194.2019.1605071.
- [81] C. H. Maeng *et al.*, “Comparison of Total Body Irradiation (TBI) Conditioning with Non-TBI for Autologous Stem Cell Transplantation in Newly Diagnosed or Relapsed Mature T- and NK-Cell Non-Hodgkin Lymphoma,” *Cancer Res. Treat.*, vol. 49, no. 1, pp. 92–103, Jan. 2017, doi: 10.4143/crt.2015.476.
- [82] G. Grabowski, M. J. Pacana, and E. Chen, “Keloid and Hypertrophic Scar Formation, Prevention, and Management: Standard Review of Abnormal Scarring in Orthopaedic Surgery,” *J. Am. Acad. Orthop. Surg.*, vol. 28, no. 10, pp. e408–e414, May 2020, doi: 10.5435/JAAOS-D-19-00690.
- [83] H. Safigholi *et al.*, “Update of the CLRP TG-43 parameter database for low-energy brachytherapy sources,” *Med. Phys.*, vol. 47, no. 9, pp. 4656–4669, Sep. 2020, doi: 10.1002/MP.14249.
- [84] Y.-F. F. Wang, S.-C. C. Lin, Y. H. Na, P. J. Black, and C.-S. S. Wu, “Dosimetric verification and commissioning for a small animal image-guided irradiator,” *Phys. Med. Biol.*, vol. 63, no. 14, p. 145001, Jul. 2018, doi: 10.1088/1361-6560/aacded.
- [85] N. Lamichhane, V. N. Patel, and M. T. Studenski, “Going the distance: validation of Acuros and AAA at an extended SSD of 400 cm,” *J. Appl. Clin. Med. Phys.*, vol. 17, no. 2, pp. 63–73, 2016.
- [86] N. Lamichhane and M. T. Studenski, “Improving TBI lung dose calculations: Can the treatment planning system help?,” *Med. Dosim.*, vol. 45, no. 2, pp. 168–171, 2019, doi: 10.1016/j.meddos.2019.09.004.

- [87] A. Hussain, E. Villarreal-Barajas, D. Brown, and P. Dunscombe, “Validation of the Eclipse AAA algorithm at extended SSD,” *J. Appl. Clin. Med. Phys.*, vol. 11, no. 3, pp. 90–100, 2010, doi: 10.1120/jacmp.v11i3.3213.
- [88] T. E. Tyson, M. B. Podgorsak, A. K. Singh, and I. Z. Wang, “Improved dose homogeneity using electronic compensation technique for total body irradiation,” *J. Appl. Clin. Med. Phys.*, vol. 19, no. 3, pp. 159–167, May 2018, doi: 10.1002/acm2.12316.





**TURUN  
YLIOPISTO**  
UNIVERSITY  
OF TURKU

ISBN 978-951-29-9209-6 (PRINT)  
ISBN 978-951-29-9210-2 (PDF)  
ISSN 0082-7002 (Print)  
ISSN 2343-3175 (Online)